J. theor. Biol. (1993) **163,** 277–314

Dynamics and Control of Bipedal Locomotion

TAD MCGEER

The Insitu Group, 224 Robin Way, Menlo Park, CA 94025, U.S.A.

(*Received on* 19 *September* 1991, *Accepted in revised form on* 16 *December* 1992)

The human frame is built for walking. It has both the right kinematics and the right dynamics—so much so, in fact, that our legs are capable of walking without any motor control. Their gait can be sustained simply by interaction of gravity and inertia, in a natural limit cycle which we call *passive dynamic walking*. This cycle needs motor input only for starting and stopping, for modulation when terrain calls for irregular strides, and for energy supply when the need arises. Analytical study reveals that any of several simple control strategies are effective for these purposes. This helps to explain why dextrous and efficient walking is so easy to a child to master. Moreover, it suggests that rehabilitation and robot design may be less difficult than one might at first imagine.

1. Passive Locomotion Cycles

We offer here a theory of legged locomotion based upon the phenomenon of *passive dynamic walking*. The treatment extends our earlier work on gravity-powered models (McGeer, 1990*b*) to encompass walking on up- and downhill grades, over a range of speeds, and with modulation of the gait to accommodate uneven footholds. At the same time, it provides a detailed mathematical companion to our somewhat lighter treatment in McGeer (1992). It is intended for mathematically inclined readers with interest in either animal locomotion or robot design.

To begin on familiar ground, we cite the toy of Fig. 1. It walks passively, that is to say, without any motor control. Energy is obtained by descending a shallow slope, and the gait emerges as a naturally stable limit cycle. The same effect is inherent in quite a variety of other models, and so can form the basis for legged locomotion in many forms. Take, for example, the range of possibilities illustrated in Fig. 2(a)–(h). Models (a) and (b) are "silly wheels" which we will use to illustrate key concepts and mathematical methods. Models (c), (d) and (e) are straight-legged bipeds similar to the toy: model (c) is the simplest, consisting of just an isolated pair of legs confined to the sagittal plane. Model (d) adds an (actively balanced) torso, while model (e) has a hip joint of finite width and moves in three dimensions. Model (f) is a knee-jointed passive walker, which is particularly attractive because it has a strikingly anthropomorphic gait. Finally, models (g) and (h) extend the passive dynamic idea to running and hopping, using springs in the legs and hip as cyclic energy stores. [The action of various natural tissues with the necessary spring-like properties has been noted by Alexander (1988).] We will use the first four of these models to study the dynamics of

0022–5193/93/015277+38 $08.00/0

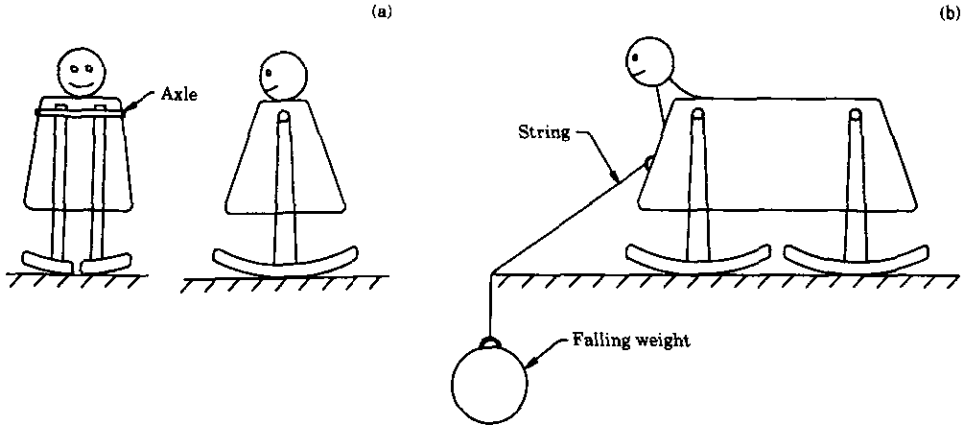

FIG. 1. A bipedal toy which walks passively down shallow inclines (from McMahon, 1984). Quadrupedal toys of similar design walk passively on level ground while being drawn by a falling weight.

fully passive walking, and the pumping and modulation of these dynamics to achieve dextrous locomotion. Details of the remaining models can be found in the references. All symbols, sub- and superscripts are defined in Appendices A and B, respectively.

Now consider, informally at first, how passive cycles can be calculated. Take the start of a cycle to be the instant when the trailing leg leaves the ground. At this point each model has certain degrees of freedom. For example, the straight-legged biped (c) has three: the rotational speeds of the two legs Ω_C and Ω_F, plus the inter-leg angle 2α. (Individual leg angles are $\pm\alpha$.) If these are specified then the subsequent motion is determined, and proceeds generally as shown in Fig. 2. [Note that this model runs the risk of dragging its swing foot at midstride. Consequently, when testing robots of this type we either folded the swing foot out of the way or arranged the floor as a chequerboard pattern of stepping stones (McGeer, 1990*b*). Knee-jointed models do not have this problem.] After getting through midstride the swing foot eventually hits the ground; there is then an impulsive energy loss, and an effectively instantaneous change in rotational speeds as support is transferred fron one leg to the next. This leaves the model ready to begin the next stride. If the angles and speeds at this instant are the same as they were at the beginning of the preceding stride, then the walking cycle is re-entrant and will repeat indefinitely.

The knee-jointed walker illustrates the same idea in a more complicated cycle. Its stance knee rests against a mechanical stop and so moves as a single unit throughout the cycle. Meanwhile, however, the swing knee starts in flexural rotation, so the swing shank and thigh move independently. This continues until the knee rotates back to full extension towards the end of the stride, whereupon impact occurs against the mechanical stop and the impulse changes the speed of each link. After that both knees remain extended until heel strike, when there is another collision and another shift in speeds. Again, if this chain of events leaves the initial conditions the same as on the previous stride, then the cycle repeats indefinitely.

In mathematical terms there is, in general, a *stride function* S that maps initial

conditions v from one stride to the next:

$$v_{k+1} = S(v_k). \tag{1}$$

For a cyclic gait we must find an argument v_0 which maps onto itself:

$$v_0 = S(v_0). \tag{2}$$

Formulation of S is relatively simple for the "silly wheels" of Fig. 2(a) and (b), so we will discuss them first to demonstrate the idea (sections 3, 6). Then we will develop more general mathematics for straight-legged biped walking.

2. Stability of Passive Cycles

To be successful a passive mechanism must have not only a cyclic gait, but also the ability to recover when the gait is disturbed. Recovery from all possible disturbances would be too much to ask, but small perturbations should be tolerable. This level of stability can be investigated by linearizing the stride function (1). We take the cyclic start-of-stride conditions v_0 as the reference point for linearization. Then

$$S(v_0+\Delta v) \approx S(v_0)+\nabla S\,\Delta v \tag{3}$$

∇S is the gradient matrix of S, evaluated at v_0 [for example, (67)], and Δv is the perturbation in start-of-stride conditions. Then the stride-to-stride mapping (1) is approximately

$$v_0+\Delta v_{k+1} \approx S(v_0)+\nabla S\,\Delta v_k. \tag{4}$$

Canceling the cyclic terms (2) leaves

$$\Delta v_{k+1} \approx \nabla S\,\Delta v_k. \tag{5}$$

This is just a set of linear difference equations. Therefore transients following small perturbations can be analyzed into modes of the form

$$\Delta v_k \sim v_z z^k \tag{6}$$

where z is an eigenvalue of ∇S, and v_z the associated eigenvector. For stability, all eigenvalues must have magnitude less than unity, with smaller magnitudes indicating that fewer strides are required to recover from a disturbance.

Table 1 lists eigenvalues and eigenvectors for the two-dimensional biped models. The precise numerical values depend upon each model's mass distribution and other parameters, and in some cases instabilities can arise. However, the remarkable point is that passive cycles are stable over a wide range of parameter choices, which implies that walking and running are easier than standing still (standing being impossible without active balance). Note also that similar modes can be recognized from one model to the next. Hence if we use the simple "silly wheels" to develop analysis and interpretation of transient behavior, then the understanding that emerges can be transferred directly to the more complicated cases.

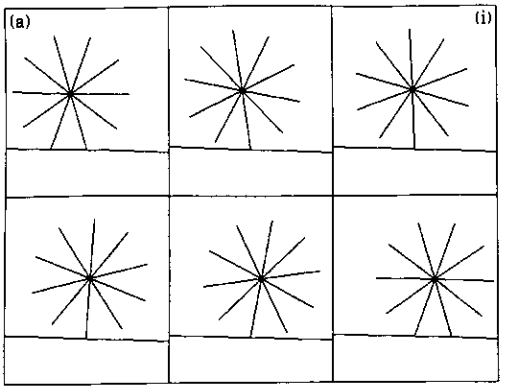
(a)
(i)

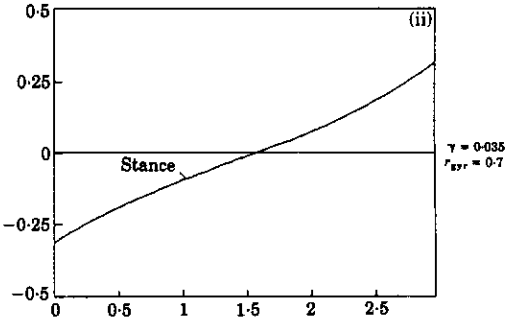
(ii)
0·5
0·25
0
−0·25
−0·5
0
0·5
1
1·5
2
2·5
Stance
γ = 0·035
r_{EXT} = 0·7

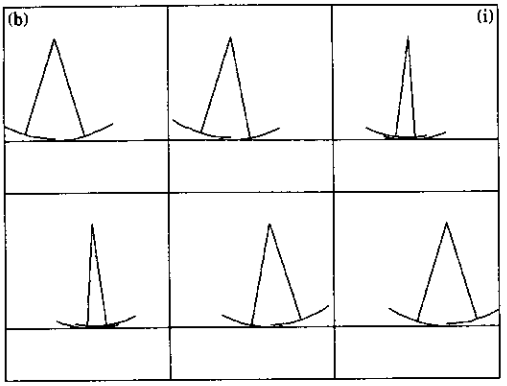
(b)
(i)

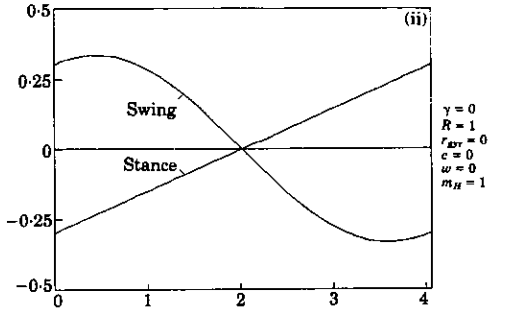
(ii)
0·5
0·25
0
−0·25
−0·5
0
1
2
3
4
Swing
Stance
γ = 0
R = 1
r_{EXT} = 0
c = 0
w = 0
m_H = 1

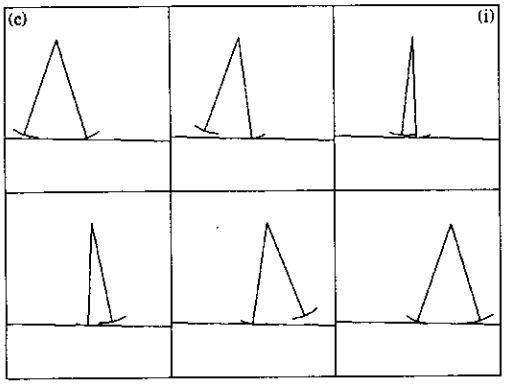
(c)
(i)

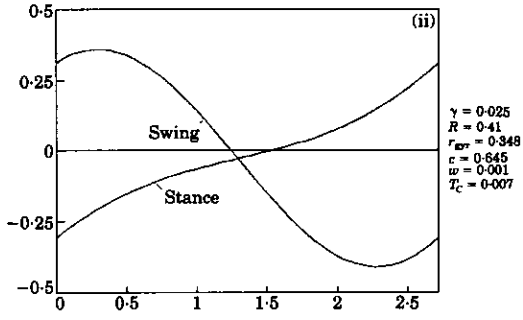
(ii)
0·5
0·25
0
−0·25
−0·5
0
0·5
1
1·5
2
2·5
Swing
Stance
γ = 0·025
R = 0·41
r_{EXT} = 0·348
c = 0·645
w = 0·001
T_C = 0·007

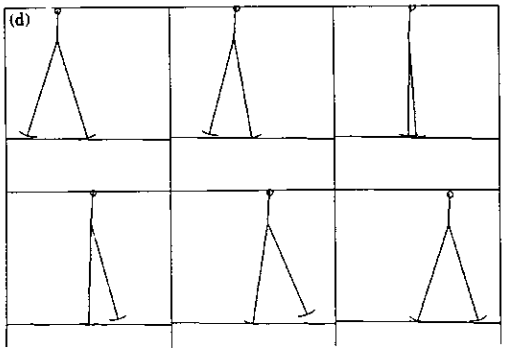
(d)

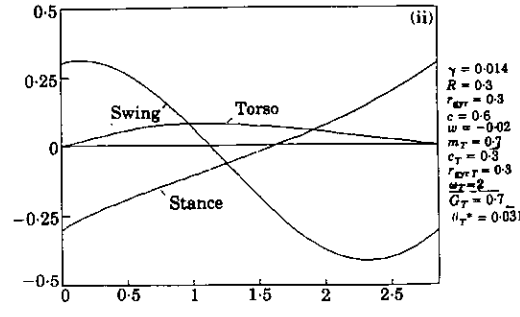
(ii)
0·5
0·25
0
−0·25
−0·5
0
0·5
1
1·5
2
2·5
Swing
Torso
Stance
γ = 0·014
R = 0·3
r_{EXT} = 0·3
c = 0·6
w = −0·02
m_T = 0·7
c_T = 0·3
r_{EXT} = 0·3
$\frac{\omega_T^2}{G_T}$ = 0·7
I_T^* = 0·031

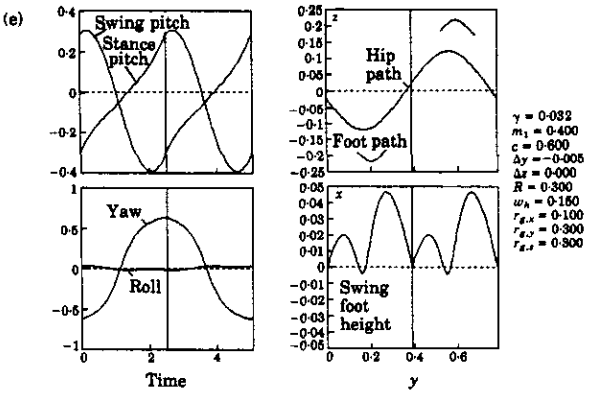
(e)
Swing pitch
Stance pitch
Yaw
Roll
Time
Hip path
Foot path
Swing foot height
y
γ = 0·032
m1 = 0·400
c = 0·600
Δy = −0·005
Δx = 0·000
R = 0·300
wh = 0·150
rg.x = 0·100
rg.y = 0·300
rg.z = 0·300

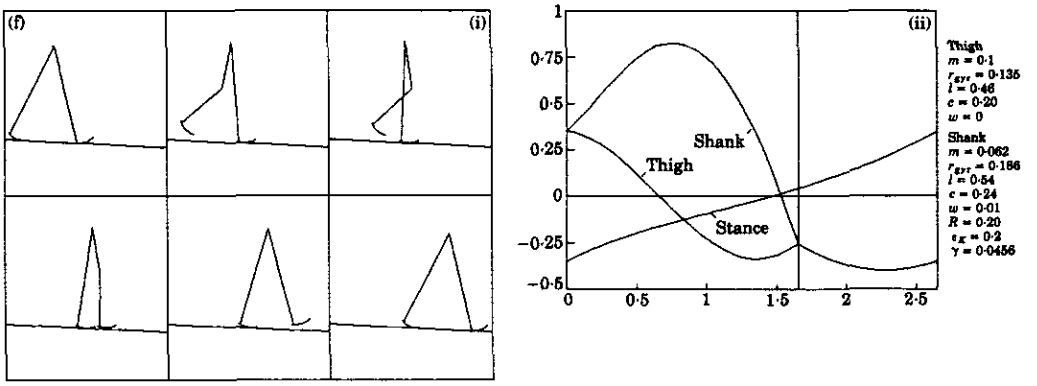
(f)
(i)
(ii)
Shank
Thigh
Stance
Thigh
m = 0·1
rgyr = 0·135
l = 0·46
c = 0·20
w = 0
Shank
m = 0·062
rgyr = 0·186
l = 0·54
c = 0·24
w = 0·01
R = 0·20
eK = 0·2
γ = 0·0456

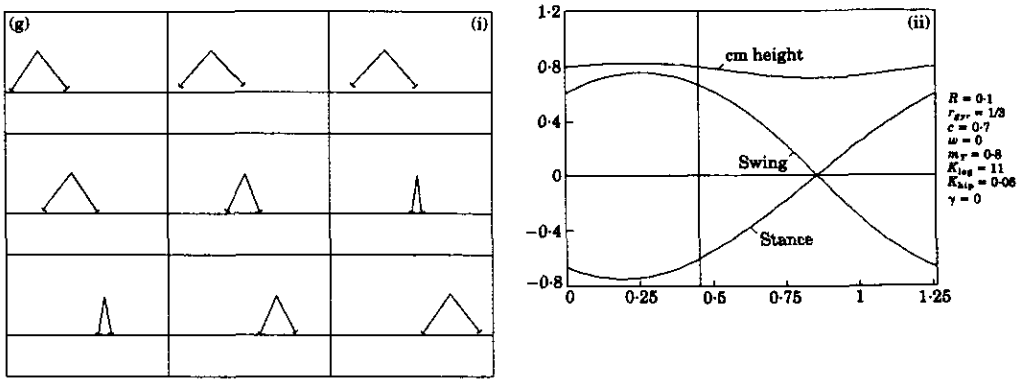
(g)
(i)
(ii)
cm height
Swing
Stance
R = 0·1
rgyr = 1/3
c = 0·7
w = 0
mT = 0·8
Kleg = 11
Khip = 0·06
γ = 0

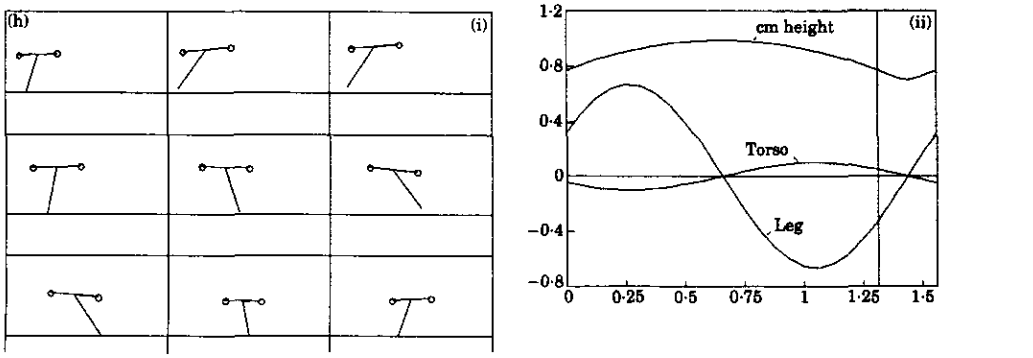
(h)
(i)
(ii)
cm height
Torso
Leg

TABLE 1

Stride-to-stride eigenvectors of typical passive cycles. Elements are normalized as appropriate by leg length l *and gravitational acceleration* g. *Each eigenvector also has been scaled so that its largest element has unit value*

Rimless wheel (McGeer, 1990*b*)			
Mode	Speed		
Eigenvalue, z	η^2		
Ω_C	1		
Walking wheel (McGeer, 1990*b*)			
Mode	Speed	Swing	Totter
Eigenvalue, z	1	0	−0·2
α	$2{\cdot}03/\omega_F$	$2/\omega_F$	1
Ω_C	1	0	0
Ω_F	1	1	0

FIG. 2. (a)–(h) illustrate typical cyclic gaits for various passive models. Except as noted, link angles relative to the surface normal are shown vs. time. Timescales are normalized by $\sqrt{l/g}$. (a) Rimless wheel (McGeer, 1990*b*). On a sufficiently steep slope (here 0·035 rad), it establishes a cyclic rolling motion, with energy gained from descent through each stride balancing energy dissipated in an inelastic collision at heel strike. (b) Walking wheel (McGeer, 1990*b*). This is the simplest of bipeds, whose legs are two spokes and feet two rim sections from an ordinary wheel. It has a large mass at the hip to decouple the stance and swing motions. Thus one leg behaves as a section of wheel, rotating along the ground at constant speed, and the other as a pendulum, swinging forward in preparation for the next stride. The legs exchange roles when they reach opposite angles. The cycle continues indefinitely, mimicking a rolling wheel. (c) Straight-legged biped walker (McGeer, 1990*b*). This is a more general version of the walking wheel, with smaller feet and more flexibility in the mass distribution. Like a rimless wheel it dissipates energy at heel strike, and so needs a shallow downhill slope to keep the cycle going. (d) Straight-legged biped with actively-stabilized torso (McGeer, 1988). Here a torso is added to the previous model. The torso is an inverted pendulum and so requires active stabilization; this is provided by a damped spring acting against the stance leg. Meanwhile the legs continue to walk passively. (e) Straight-legged biped with a three-dimensions cycle (McGeer, 1991). Side-to-side swerving is superimposed upon a longitudinal motion which is essentially the same as in two dimensions. Swerving allows the weight of the swing leg (here offset from the stance leg by 0·15*l*) to be balanced by centrifugal effect about the vertical axis. Humans maintain a more nearly straight motion by rotating their legs toward the body centerline while walking, but this example illustrates the possibility of a three-dimensional passive motion with a simpler model. As in two-dimensional, the swing foot is calculated to pass slightly below ground level at midstride, but this problem would be remedied by knees. (f) Knee-jointed biped walker (Mochon & McMahon, 1980; McGeer, 1992). Passive walking also works with knee-jointed legs. The knees have mechanical stops to prevent hyperextension; with the feet placed forward on the leg, the contact force then keeps the stance knee locked throughout the stride. Meanwhile the swing leg flexes naturally, re-extends after midstride, locks inelastically when the knee reaches full extension, and thereafter remains extended until heel strike. This cycle is appealingly anthropomorphic, and also has the practical advantage of passive foot clearance. (g) Biped runner (McGeer, 1990*a*). Running can be realized by putting a torsional spring at the hip and telescoping springs in each leg. The torsional spring gives the legs a natural "scissor" oscillation, and the telescoping springs allow for bouncing between stance and flight phases. The cyclic gait is essentially a combination of these two motions proceeding in-phase. (h) Monoped hopper (Thompson & Raibert, 1989). The "bounce-and-scissor" cycle of the biped runner can also be realized in a monoped. Here the scissoring spring is put between the leg and torso.

TABLE 1—continued.

Straight-legged biped walker (McGeer, 1990*b*)

Mode	Speed	Swing	Totter
Eigenvalue, z	0·70	−0·05	−0·83
α	0·88	0·14	1
Ω_C	1	0·15	0·13
Ω_F	0·27	1	−0·03

Knee-jointed biped walker (McGeer, 1990*c*)

			Totter	
Mode	Speed	Swing	Mag.	±Phase
Eigenvalue, z	0·07	−0·002	0·45	±0·95
α	0·17	0·08	0·38	±0·00
Ω_C	0·11	0·06	0·28	±0·57
Ω_{FT}	−0·97	−0·19	0·89	±2·82
Ω_{FS}	1	1	1	±0

Straight-legged biped walker with actively stabilized torso (McGeer, 1988)

			Totter		
Mode	Speed	Swing	Mag.	±Phase	Torso
Eigenvalue, z	0·47	0·0015	0·18	±2·62	$1·6 \times 10^{-5}$
α	1	0·01	0·62	±2·48	0·07
θ_T	−0·16	−0·47	0·13	∓2·91	−0·49
Ω_C	0·60	0·32	0·60	±2·80	−0·16
Ω_F	−0·31	1	0·50	∓3·08	0·29
Ω_T	0·90	−0·59	1	±0	1

Biped runner (McGeer, 1990*a*)

		Swing		Totter	
Mode	Speed	Mag.	±Phase	Mag.	±Phase
Eigenvalue, z	1	0·22	±1·62	1·65	±2·42
θ_C	−0·18	0·03	±1·43	0·08	∓0·55
θ_F	0·11	0·49	∓2·99	0·24	∓2·60
Ω_C	−0·58	0·08	∓1·02	0·14	∓1·61
Ω_F	1	1	±0	1	±0
l_C	−0·73	0·09	±1·84	0·15	±1·04

3. The Rimless Wheel

Having reviewed in the abstract all of the elements of passive walking analysis, let us take up the specific case of the rimless wheel. First we develop its stride function (1). In cases of interest the stance leg angle θ_C remains small throughout, so the equation of motion can be written as

$$\frac{d^2\theta_C}{dt^2} - \sigma^2\theta_C \approx \sigma^2\gamma. \tag{7}$$

Here θ_C is measured from the surface normal. All quantities are normalized by total mass m, leg length l, and gravity g. σ is a dimensionless pendulum frequency, given by

$$\sigma^2 \equiv \frac{1}{1+r_{gyr}^2} \tag{8}$$

where r_{gyr} is the wheel's radius of gyration about the hub. Start-of-stride conditions are

$$\theta_C(0) = -\alpha_0, \qquad \Omega_C(0) = \Omega_{C_k}. \tag{9}$$

The motion during the stride, found by solving (7), then satisfies

$$\theta_C(\tau) = \frac{1}{2}(\gamma - \alpha_0 + \Omega_{C_k}/\sigma)e^{\sigma\tau} + \frac{1}{2}(\gamma - \alpha_0 - \Omega_{C_k}/\sigma)e^{-\sigma\tau} - \gamma \tag{10}$$

$$\Omega_C(\tau) = \frac{\sigma}{2}(\gamma - \alpha_0 + \Omega_{C_k}/\sigma)e^{\sigma\tau} - \frac{\sigma}{2}(\gamma - \alpha_0 - \Omega_{C_k}/\sigma)e^{-\sigma\tau}. \tag{11}$$

The motion proceeds until $\theta_C = \alpha_0$, when the next leg strikes the ground. Applying this condition determines the stride period and end-of-stride speed:

$$e^{\sigma\tau_k} = \frac{\gamma + \alpha_0 + \sqrt{(\Omega_{C_k}/\sigma)^2 + 4\gamma\alpha_0}}{\gamma - \alpha_0 + \Omega_{C_k}/\sigma} \tag{12}$$

$$\Omega_C(\tau_k) = \sqrt{\Omega_{C_k}^2 + 4\gamma\alpha_0\sigma^2}. \tag{13}$$

We treat the collision as inelastic and impulsive. In that case the wheel conserves angular momentum about the impact point, and the loss in speed can be calculated as follows. The angular momenta immediately before and after impact are

$$H^- = (\cos 2\alpha_0 + r_{gyr}^2)ml^2\Omega_C(\tau_k) \tag{14}$$

$$H^+ = (1 + r_{gyr}^2)ml^2\Omega_{C_{k+1}}. \tag{15}$$

Equating these implies that

$$\Omega_{C_{k+1}} = \frac{\cos 2\alpha_0 + r_{gyr}^2}{1 + r_{gyr}^2}\Omega_C(\tau_k) \equiv \eta\Omega_C(\tau_k). \tag{16}$$

Notice that η is a measure of the wheel's efficiency. Substituting for $\Omega_C(\tau_k)$ from (13) produces the stride function:

$$\Omega_{C_{k+1}} = \eta\sqrt{\Omega_{C_k}^2 + 4\gamma\alpha_0\sigma^2}. \tag{17}$$

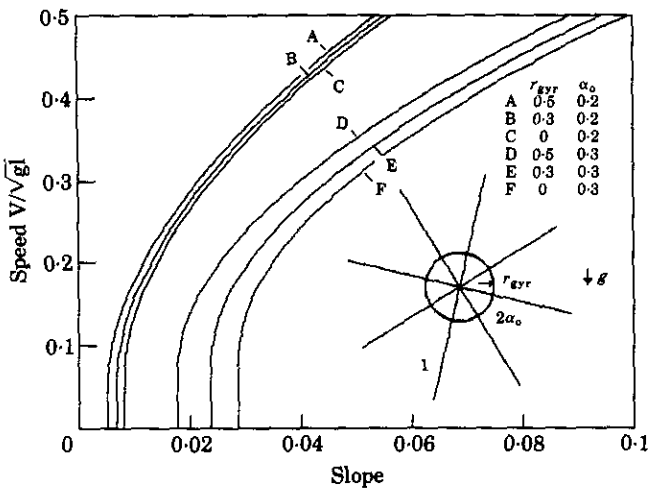

FIG. 3. Speed of a rimless wheel rolling downhill (expressed in units of $\sqrt{gl}$). Larger inertia and smaller step length produce higher speeds.

Now we can find the steady cycle. The cyclic-gait condition is that $\Omega_{C_{k+1}} = \Omega_{C_k} = \Omega_{C_0}$; inserting this into the stride function leads to

$$\Omega_{C_0} = \sqrt{\frac{4\gamma\alpha_0\sigma^2\eta^2}{1-\eta^2}}. \tag{18}$$

The corresponding forward speed, averaged over the stride, is

$$V_O = \frac{2\alpha_0}{\tau_0} \tag{19}$$

with τ_0 from (12). This is plotted in Fig. 3, as a function of slope.

Next, consider small perturbations on the cyclic motion. Differentiating the stride function gives

$$\frac{d\Omega_{C_{k+1}}}{d\Omega_{C_k}} = \eta \frac{\Omega_{C_k}}{\sqrt{\Omega_{C_k}^2 + 4\gamma\alpha_0\sigma^2}}. \tag{20}$$

The value at $\Omega_{C_k} = \Omega_{C_0}$ is

$$\frac{d\Omega_{C_{k+1}}}{d\Omega_{C_k}} = \eta^2. \tag{21}$$

Hence a perturbation would decay over k strides according to

$$\Delta\Omega_{C_k} = \eta^{2k}\,\Delta\Omega|_{k=0}. \tag{22}$$

We call this transient the *speed mode*: a monotonic convergence to the speed appropriate for the slope in use. The more efficient the wheel, the more strides are necessary for convergence. All of the models in Table 1, despite their obviously more complicated dynamics, have a mode with similar behavior.

4. Impulsive Pushing

The rimless wheel, in addition to serving as a simplified model for gravity-powered walking, offers an easily understood introduction to alternative methods of energy supply. We will consider two possibilities. One is analogous to pushing with the stance knee in human walking, which is particularly useful for climbing stairs. The other is analogous to plantarflexion of the stance angle, which generates a push from the trailing foot as it leaves the ground. We will study the plantarflexion method first.

For analytical convenience we will concentrate the push into an impulse applied at the point of contact. Nominally the impulse and support transfer will be simultaneous, but we will demonstrate that energy consumption depends strongly upon the sequencing of the two events. Suppose first that the impulse ($\boldsymbol{P}_{k+1}$) is applied just before contact of the forward foot, in which case it actually makes the wheel jump off the ground. Initial velocities in rotation and translation for the flight phase are

$$V_{CM_f} = V_{CM}(\tau_k) + \boldsymbol{P}_{k+1} = \begin{bmatrix} -\sin\alpha_0 \\ \cos\alpha_0 \end{bmatrix} \Omega_C(\tau_k) + \boldsymbol{P}_{k+1} \tag{23}$$

$$\Omega_{C_f} = \Omega_C(\tau_k) + \frac{1}{r_{gyr}^2}[\sin\alpha_0 - \cos\alpha_0]\boldsymbol{P}_{k+1}. \tag{24}$$

If the impulse is smaller than a certain limit, then it slows but does not stop the downward motion of the forward leg, and the jump off one foot is followed immediately by landing on the next. This event produces another impulse $\boldsymbol{P}_h$ and another change in velocities, satisfying

$$V_{CM_{k+1}} = \begin{bmatrix} \sin\alpha_0 \\ \cos\alpha_0 \end{bmatrix} \Omega_{C_{k+1}} = V_{CM_f} + \boldsymbol{P}_h \tag{25}$$

$$\Omega_{C_{k+1}} = \Omega_{C_f} - \frac{1}{r_{gyr}^2} \boldsymbol{P}_h^T \begin{bmatrix} \sin\alpha_0 \\ \cos\alpha_0 \end{bmatrix}. \tag{26}$$

Define

$$\Gamma \equiv \frac{2\sin\alpha_0}{1 + r_{gyr}^2}. \tag{27}$$

Then eliminating V_{CM} and $\boldsymbol{P}_h$ from (23–26) leaves

$$\Omega_{C_{k+1}} = \eta\Omega_C(\tau_k) + \Gamma P_{x_{k+1}} \tag{28}$$

where subscript x designates the x-component of the impulsive push. This is a more general version of the original support-transfer eqn (16). The corresponding stride function [cf. (17)] becomes

$$\Omega_{C_{k+1}} = \eta\sqrt{\Omega_{C_k}^2 + 4\gamma\alpha_0\sigma^2} + \Gamma P_{x_{k+1}}. \tag{29}$$

Applying the cyclic-gait condition (2) then determines the impulse necessary for steady rolling on any selected slope and speed:

$$P_{x_0} = \frac{1}{\Gamma}(\Omega_{C_0} - \eta\sqrt{\Omega_{C_0}^2 + 4\gamma\alpha_0\sigma^2}). \tag{30}$$

Now let us evaluate the energy supplied. In the impulsive limit the product of force and displacement during the push is

$$W = \boldsymbol{P}^T \tfrac{1}{2}(\boldsymbol{V}_p^- + \boldsymbol{V}_p^+) \tag{31}$$

where $\boldsymbol{V}_p^-$ and $\boldsymbol{V}_p^+$ are the velocities of the trailing foot immediately before and after the impulse is applied. If the push precedes support transfer, then $\boldsymbol{V}_p^-$ is zero, and

$$\boldsymbol{V}_p^+ = \boldsymbol{V}_{CM_f} + \begin{bmatrix} \sin\alpha_0 \\ -\cos\alpha_0 \end{bmatrix} \Omega_{C_f}. \tag{32}$$

On the other hand, if the impulse follows support transfer, then it turns out that the equation for support transfer (28) still holds; however, the velocities in (31) become

$$\boldsymbol{V}_p^+ = 2\sin\alpha_0 \Omega_{C_{k+1}} \hat{\boldsymbol{x}} \tag{33}$$

$$\boldsymbol{V}_p^- = 2\sin\alpha_0 (\Omega_{C_{k+1}} - \Gamma P_{x_{k+1}}) \hat{\boldsymbol{x}}. \tag{34}$$

The energy inputs then work out to

$$\text{Pre-ST } W = \tfrac{1}{2}\boldsymbol{P}_{k+1}^T \left(\boldsymbol{P}_{k+1} + \frac{1}{r_{\text{gyr}}^2} \begin{bmatrix} \sin^2\alpha_0 & -\sin\alpha_0\cos\alpha_0 \\ -\sin\alpha_0\cos\alpha_0 & \cos^2\alpha_0 \end{bmatrix} \boldsymbol{P}_{k+1} \right) \tag{35}$$

$$\text{Post-ST } W = P_{x_{k+1}} \left(\frac{\Omega_{C_{k+1}}}{\sigma} - \frac{\sin\alpha_0}{1 + r_{\text{gyr}}^2} P_{x_{k+1}} \right) 2\sin\alpha_0. \tag{36}$$

Figure 4 plots these equations, as functions of slope, for steady rolling at speed $0{\cdot}25\sqrt{gl}$. Two additional functions are plotted for reference. One is just the work against gravity, which for small γ and α_0 is

$$W = -2\alpha_0\gamma. \tag{37}$$

The other is the same function offset by γ_g, the slope for gravity-powered rolling at the specified speed. If the dissipation at foot strike were invariant with slope, then energy requirements would be as indicated by this second line. However the push softens the blow, so that energy requirements for climbing prove to be smaller. Indeed if the impulse precedes support transfer then the reduction is quite dramatic, to the point that on slope $-\gamma_g$ (i.e. opposite to that for gravity-powered rolling) *dissipation goes to zero.* All of the work is applied to lifting the center of mass.

There is, as you might expect, an underlying symmetry: the dissipation-free climb is the mirror image of the gravity-powered descent. (If you were shown a film of the motion, you could not tell whether the projector was running in forward or reverse.) Naturally some care must be exercised to achieve this ideal; in particular, the climb impulse must be applied at the correct angle. From (25), (26), its components should be in the ratio

$$\frac{P_y}{P_x} = \frac{-1}{\tan\alpha_0} \frac{1-\eta}{1+\eta}. \tag{38}$$

Fortunately, as we will show presently, imprecision entails only a modest penalty.

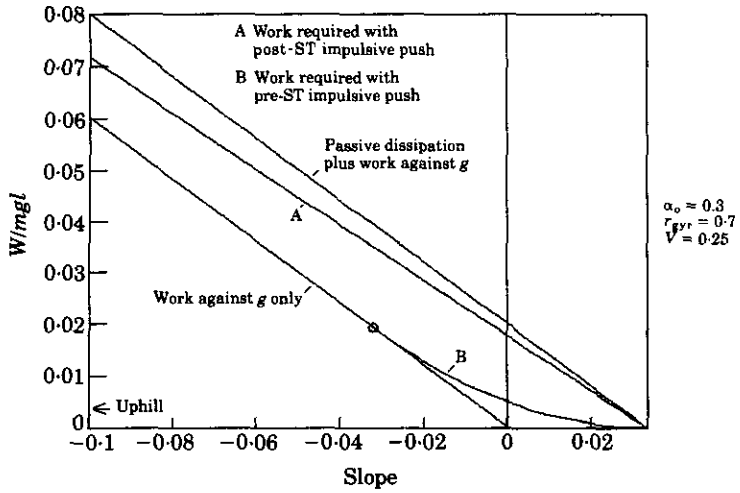

FIG. 4. Rolling of a rimless wheel can be sustained in a climb by pushing with the trailing foot just as it leaves the ground. The ordinate shows the energy input required per stride to maintain rolling at a speed of $0.25\sqrt{gl}$. The input is zero at the right-hand side of the plot, where energy gained in descending slope γ_g (here 0·033 rad) balances dissipation at heel strike. For "uphill" slopes (i.e. $\gamma < \gamma_g$) some input is required to maintain the energy balance, but the economics are sensitive to timing. In particular, much less work is required if the push is applied just before support transfer rather than just after.

Dissipation is eliminated by this ideal impulse because it is just strong enough to arrest the forward foot before it hits the ground. But by the same token, a slightly stronger impulse would launch the wheel right off the ground. This precludes applying the same strategy for steeper climbs at the same speed, so, instead, one must adopt one of the following alternatives:

(i) Go faster. According to the symmetry argument, the speed for dissipation-free climbing increases with slope according to the mirror image of Fig. 3. However, this strategy carries the rather odd corollary that higher efficiency calls for a bigger engine.

(ii) Push more gradually. The wheel will not be thrown off the gound if the impulse is delivered sufficiently slowly that the peak force is only of order *mg*.

(iii) Combine pushing with leg length variation (analogous to knee flexure).

On steep slopes the last of these is the only practical choice, and we will discuss it further below. However, let us first finish impulse-powered rolling with a brief stability analysis. Applying the general procedure (5) to the stride function (29) produces

$$\Delta\Omega_{C_{k+1}} \approx \eta \frac{\Omega_{C_0}}{\sqrt{\Omega_{C_0}^2 + 4\gamma\alpha_0\sigma^2}} \Delta\Omega_{C_k} + \Gamma\Delta P_{x_{k+1}}. \tag{39}$$

The coefficient of $\Delta\Omega_{C_k}$ increases in a climb, reaching unity when $\gamma = -\gamma_g$. This implies that perfectly efficient climbing without active control would be neutrally stable. Stability could be improved by varying the pulse according to a simple

feedback law:

$$\Delta P_{x_{k+1}} = K(\Omega_{C_0} - \Omega_{C_k}) \tag{40}$$

where K is selected to produce any desired speed-mode eigenvalue z, according to

$$K = \frac{1}{\Gamma}\left(\eta \frac{\Omega_{C_0}}{\sqrt{\Omega_{C_0}^2 + 4\gamma\alpha_0\sigma^2}} - z\right). \tag{41}$$

5. Length Cycling

Our second scheme for "pumping" the passive motion involves leg length variation. Humans do this by knee flexure, but for the rimless wheel we instead imagine a telescopic action. The stance leg starts the stride with length $(1-\Delta l)$, lengthens instantaneously to $(1+\Delta l)$ while passing through the vertical, and then continues at this length until support transfer. Start- and end-of-stride angles with this strategy satisfy

$$(1-\Delta l)\cos\theta_i = (1+\Delta l)\cos\theta_f \tag{42}$$

$$\theta_f - \theta_i = 2\alpha_0. \tag{43}$$

Formulation of the stride function is simplified if the energy E, rather than the speed Ω_C, is used as the state variable. Thus the k-th stride begins with energy

$$E_k = (1-\Delta l)\cos(\gamma+\theta_i) + \tfrac{1}{2}(r_{gyr}^2 + (1-\Delta l)^2)\Omega_{C_k}^2. \tag{44}$$

The wheel rolls to the vertical ($\theta_C = -\gamma$), decelerating to

$$\Omega_C|_{\theta_C+\gamma=0^-} = \sqrt{2\frac{E_k-(1-\Delta l)}{r_{gyr}^2+(1-\Delta l)^2}}. \tag{45}$$

Then the leg extends. Angular momentum about the foot is conserved, so the speed immediately after the length change is

$$\Omega_C|_{\theta_C+\gamma=0^+} = \frac{r_{gyr}^2+(1-\Delta l)^2}{r_{gyr}^2+(1+\Delta l)^2}\Omega_C|_{\theta_C+\gamma=0^-}. \tag{46}$$

The total energy after the length change is therefore [from (45)]

$$\begin{aligned} E_k + W &= (1+\Delta l) + \tfrac{1}{2}(r_{gyr}^2+(1+\Delta l)^2)\Omega_C^2|_{\theta_C+\gamma=0^+} \\ &= (1+\Delta l) + \frac{r_{gyr}^2+(1-\Delta l)^2}{r_{gyr}^2+(1+\Delta l)^2}(E_k-(1-\Delta l)). \end{aligned} \tag{47}$$

Then rolling on to the end-of-stride accelerates the wheel to

$$\Omega_C(\tau_k) = \sqrt{2\frac{E_k+W-(1+\Delta l)\cos(\gamma+\theta_f)}{r_{gyr}^2+(1+\Delta l)^2}}. \tag{48}$$

At support transfer angular momentum about the forward foot is conserved, so that

[cf. (14) and (15)]

$$(r_{gyr}^2+(1-\Delta l)^2)\Omega_{C_{k+1}} = (r_{gyr}^2+(1-\Delta l)(1+\Delta l)\cos 2\alpha_0)\Omega_C(\tau_k). \tag{49}$$

The coefficient of restitution η in this case [cf. (16)] is then

$$\eta = \frac{r_{gyr}^2+(1-\Delta l^2)\cos 2\alpha_0}{r_{gyr}^2+(1-\Delta l)^2}. \tag{50}$$

The energy at the start of stride $k+1$, from (44), (47), and (48), works out to

$$\begin{aligned} E_{k+1} = &\left(\frac{r_{gyr}^2+(1-\Delta l)^2}{r_{gyr}^2+(1+\Delta l)^2}\right)^2 \eta^2 E_k + (1-\Delta l)\cos(\gamma+\theta_i) \\ &- \left(\frac{r_{gyr}^2+(1-\Delta l)^2}{r_{gyr}^2+(1+\Delta l)^2}\right)^2 \eta^2(1-\Delta l) \\ &+ \frac{r_{gyr}^2+(1-\Delta l)^2}{r_{gyr}^2+(1+\Delta l)^2}\eta^2(1+\Delta l)(1-\cos(\gamma+\theta_f)). \end{aligned} \tag{51}$$

This is the stride function.

Specifying Δl and invoking the cyclic condition (2) produces a solution, but to find the corresponding translational speed we need the stride period. This is not supplied by the analysis of energetics, so instead we turn to the equation of motion (7). Length change modifies the timescale parameter σ (8); thus before and after the event we have

$$\sigma_i = \sqrt{\frac{(1-\Delta l)}{r_{gyr}^2+(1-\Delta l)^2}} \tag{52}$$

$$\sigma_f = \sqrt{\frac{(1+\Delta l)}{r_{gyr}^2+(1+\Delta l)^2}}. \tag{53}$$

Pre- and post-length-change sections of the stride must be calculated separately. The original solutions (10) and (11) apply in each section, with appropriate modifications to σ and initial angles and speeds. The stride period ultimately turns out to satisfy

$$\tau_k = \frac{1}{2\sigma_i}\ln\frac{\Omega_{C_k}/\sigma_i-\gamma-\theta_i}{\Omega_{C_k}/\sigma_i+\gamma+\theta_i} + \frac{1}{2\sigma_f}\ln\frac{\Omega_C(\tau_k)/\sigma_f+\gamma+\theta_f}{\Omega_C(\tau_k)/\sigma_f-\gamma-\theta_f} \tag{54}$$

with $\Omega_C(\tau_k)$ from (48). This, together with the stride length [from (42)], determines the wheel's translational speed.

These formulae allow calculation of energy requirements as a function of slope and speed. In Fig. 4 the results would fall just above the "gravity plus dissipation" line, indicating that dissipation increases slightly in a climb. However this penalty would be suffered only if length cycling were used on its own. When humans negotiate steep slopes, we instead use length cycling and impulsive pushing in combination; to see the advantage of this approach, consider the problem of steep descent. If the legs were held at fixed length in such a descent, then according to (18) the speed would

become intolerably high. (In fact, centrifugal effect would throw the wheel off the ground.) If, on the other hand, length cycling were used, then speed could be regulated to whatever level were desired; some energy still would be dissipated in the heel-strike impulse, and some in the length adjustment. Now imagine watching a film of this motion—in reverse. You see a steep dissipation-free climb, with an impulsive push and length change mirrored (and easily calculated) from those in the steady descent.

6. The Walking Wheel

Next we consider the simplest of all bipeds: the "walking" or "synthetic" wheel [Fig. 2(b)]. This device earns its name by synthesizing a wagon wheel from two hinged spokes, each with a section of rim. Let us suppose that it carries a payload sufficiently large to make its overall mass center practically coincident with the hip. Now observe the following:

(i) If one leg is put on level ground and given a push, then it will behave like a section of wheel and simply roll along at constant speed.

(ii) If, meanwhile, the other leg is shortened slightly, then it will swing clear of the ground as an unforced pendulum.

(iii) Support can be transferred at any time by infinitesimal length changes. Both contact points would be directly below the hub, and consequently the transfer would *not* change the translational speed of the mass center.

With these observations in mind we can develop the stride function easily. Initial conditions are

$$\begin{aligned} \Delta\theta_C &= -\alpha_k \qquad \Omega_C = \Omega_{C_k} \\ \Delta\theta_F &= \alpha_k \qquad\ \ \Omega_F = \Omega_{Fk}. \end{aligned} \tag{55}$$

Thereafter, the positions and speeds satisfy

$$\Delta\theta_C(\tau) = -\alpha_k + \Omega_{C_k}\tau \tag{56}$$

$$\Delta\theta_F(\tau) = \alpha_k \cos\omega_F\tau + \frac{\Omega_{Fk}}{\omega_F}\sin\omega_F\tau \tag{57}$$

$$\Omega_C(\tau) = \Omega_{C_k} \tag{58}$$

$$\Omega_F(\tau) = -\omega_F\alpha_k \sin\omega_F\tau + \Omega_{Fk}\cos\omega_F\tau \tag{59}$$

where ω_F is the pendulum frequency of the free leg. Let us specify that support transfer will occur when the leg angles become equal and opposite. Then from (56) and (57) the stride period τ_k satisfies

$$\alpha_k(\cos\omega_F\tau_F - 1) + \Omega_{C_k}\tau_k + \frac{\Omega_{Fk}}{\omega_F}\sin\omega_F\tau_k = 0. \tag{60}$$

Since support transfer can produce no change in the hub speed, both legs must

emerge rotating at Ω_{C_k}. Hence the complete stride function, with τ_k given by (60), is

$$\alpha_{k+1} = -\alpha_k + \Omega_{C_k}\tau_k \tag{61}$$

$$\Omega_{C_{k+1}} = \Omega_{C_k} \tag{62}$$

$$\Omega_{Fk+1} = \Omega_{C_k}. \tag{63}$$

We now impose the cyclic-gait condition (2) and solve for the repetitive initial conditions and stride period. These turn out to satisfy

$$\omega_F\tau_0 = \pi \text{ or } 4{\cdot}058 \tag{64}$$

$$\alpha_0 = \frac{\tau_0}{2}\Omega_{C_0} \tag{65}$$

$$\Omega_{F_0} = \Omega_{C_0}. \tag{66}$$

Thus there are two sets of cyclic gaits, either of which can be sustained at any speed. Higher speeds simply call for longer strides (65), while the cadence remains constant at either of the two values in (64). Of these two possible solutions, the longer period gait, is to be preferred for a couple of reasons. First, as we shall demonstrate presently, it is stable while the other is not. Second, it entails support transfer when not only the angles match but also the speeds [cf. Fig. 2(b)]. This is more in the spirit of mimicking a genuine wheel and, moreover, suggests a practical idea. The fact that the swing foot skims the ground through the whole stride makes the walking wheel hard to implement in practice. However, observe that the foot moves forward throughout the swing phase until the moment desired for support transfer, at which point it tries to reverse. Thus, if the soles of the feet were lined with cat's fur or a similarly ratchet-like material, then an experimental model just might be made to work.

To assess stability (with angle matching as the support-transfer condition) we differentiate the stride function as follows. ∇S, for (5), is

$$\begin{bmatrix} \frac{\partial\alpha_{k+1}}{\partial\alpha_k} & \frac{\partial\alpha_{k+1}}{\partial\Omega_{C_k}} & \frac{\partial\alpha_{k+1}}{\partial\Omega_{Fk}} \\ \frac{\partial\Omega_{C_{k+1}}}{\partial\alpha_k} & \frac{\partial\Omega_{C_{k+1}}}{\partial\Omega_{C_k}} & \frac{\partial\Omega_{C_{k+1}}}{\partial\Omega_{Fk}} \\ \frac{\partial\Omega_{Fk+1}}{\partial\alpha_k} & \frac{\partial\Omega_{Fk+1}}{\partial\Omega_{C_k}} & \frac{\partial\Omega_{Fk+1}}{\partial\Omega_{Fk}} \end{bmatrix} = \begin{bmatrix} -1 & \tau_k & 0 \\ 0 & 1 & 0 \\ 0 & 1 & 0 \end{bmatrix} + \begin{bmatrix} \Omega_{C_k} \\ 0 \\ 0 \end{bmatrix} \quad \begin{bmatrix} \frac{\partial\tau_k}{\partial\alpha_k} & \frac{\partial\tau_k}{\partial\Omega_{C_k}} & \frac{\partial\tau_k}{\partial\Omega_{Fk}} \end{bmatrix}. \tag{67}$$

But from (60)

$$\begin{bmatrix} \dfrac{\partial \tau_k}{\partial \alpha_k} \\ \dfrac{\partial \tau_k}{\partial \Omega_{C_k}} \\ \dfrac{\partial \tau_k}{\partial \Omega_{Fk}} \end{bmatrix} = \frac{1}{\alpha_k \omega_F \sin \omega_F \tau_k - \Omega_{C_k} - \Omega_{Fk} \cos \omega_F \tau_k} \begin{bmatrix} \cos \omega_F \tau_k - 1 \\ \tau_k \\ \dfrac{\sin \omega_F \tau_k}{\omega_F} \end{bmatrix}. \tag{68}$$

If [from (64)] $\omega_F \tau_k = \pi$, then the leading coefficient here goes to infinity; thus the shorter-period gait is (for infinitesimal perturbations) quite dramatically unstable. If $\omega_F \tau_k = 4{\cdot}058$, on the other hand, then we have

$$\begin{bmatrix} \Delta\alpha_{k+1} \\ \Delta\Omega_{C_{k+1}} \\ \Delta\Omega_{Fk+1} \end{bmatrix} = \begin{bmatrix} -0{\cdot}2 & \dfrac{2{\cdot}03}{\omega_F} & \dfrac{0{\cdot}4}{\omega_F} \\ 0 & 1 & 0 \\ 0 & 1 & 0 \end{bmatrix} \begin{bmatrix} \Delta\alpha_k \\ \Delta\Omega_{C_k} \\ \Delta\Omega_{Fk} \end{bmatrix}. \tag{69}$$

The eigenvalues and eigenvectors of this system are as listed in Table 1. We can interpret them as follows.

(i) The "speed" mode is at root the same as in the rimless wheel. But since the walking wheel is equally happy at any speed, the mode is, in this case, neutrally stable, and the eigenvector's $\Delta\alpha/\Delta\Omega_C$ ratio is given by the steady-rolling condition (65).

(ii) The "swing" mode is a rapid elimination of any perturbation in Ω_F. With a large hip mass the first support transfer makes $\Omega_F = \Omega_C$, so $z = 0$.

(iii) The "totter" mode is a transient whereby the stride length accommodates to the steady walking speed. That is, the wheel once started maintains its initial speed through all subsequent motion; however, the initial α may not be appropriate for that speed as specified in (65). In this case, α adjusts through a decaying oscillation which persists over several steps.

These same modes can be recognized in some form across the whole the spectrum of models included in Table 1. However, of the three, the totter mode is the most variable, and as mentioned earlier, some design choices make it unstable (McGeer, 1990*b*).

7. Equations of Motion for a Straight-legged Biped

We now turn to our main attraction: the general straight-legged biped as illustrated in Fig. 5. This improves upon the walking wheel, in that it allows smaller feet more flexibility in the mass distribution, and the option of a torso. If the torso is included, then some provision must be made for keeping it upright. The obvious scheme is to apply appropriate torques at the hip, with reaction against the stance leg (that offering a more robust antagonist than the swing leg). Here we will choose the torques such that the torso angle remains constant throughout the stride. This

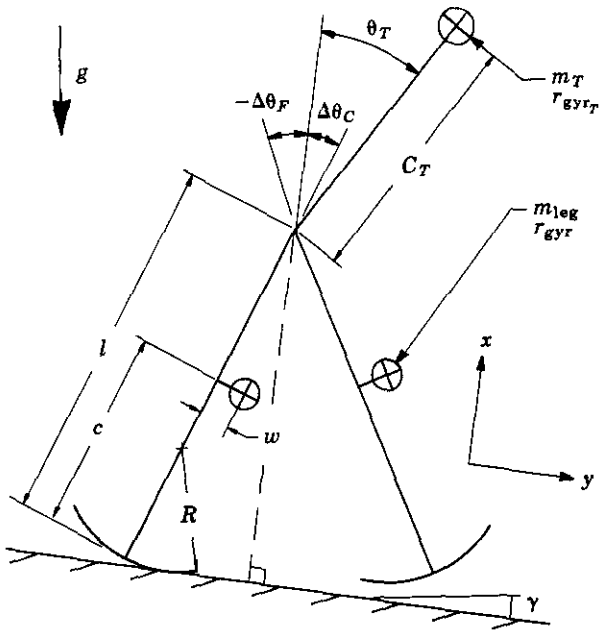

FIG. 5. General model of a straight-legged biped walker. Motion is confined to the sagittal plane. (In practice this can be arranged by building each leg like a coupled pair of crutches. See McGeer, 1990*b*.)

proves to be a good approximation for the more complicated case illustrated in Fig. 2(d), in which the torso bobs back and forth.

Analysis begins with the equations of motion. These are fourth order, with state variables

$$\boldsymbol{\theta} \equiv \begin{bmatrix} \theta_C \\ \theta_F \end{bmatrix} \tag{70}$$

$$\boldsymbol{\Omega} \equiv \begin{bmatrix} \Omega_C \\ \Omega_F \end{bmatrix}. \tag{71}$$

In straight-legged walking (although *not* in running or knee-joint walking), the angles remain near the vertical and the speeds remain small ($\ll\sqrt{g/l}$). Therefore it is reasonably safe to linearize, and write the equations of motion as

$$\mathbf{M}_0\boldsymbol{\Omega} + \mathbf{K}[\Delta\boldsymbol{\theta} - \Delta\boldsymbol{\theta}_{SE}] \approx \boldsymbol{T} \tag{72}$$

where $\Delta\boldsymbol{\theta}$ is the rotation from the surface normal, $\Delta\boldsymbol{\theta}_{SE}$ (81) the static equilibrium position, $\mathbf{K}$ (D.18) the stiffness matrix, $\mathbf{M}_0$ (D.23) the inertia matrix, and $\boldsymbol{T}$ a vector of (optional) control torques applied to each leg. The derivation of this system is given in Appendix D. Its solution can be expressed in terms of a transition matrix $\boldsymbol{D}(\tau)$ (F.4), relating the initial state to the state at time τ later in the stride. The form of this

solution is

$$\begin{bmatrix} \Delta\boldsymbol{\theta}(\tau) \\ \boldsymbol{\Omega}(\tau) \end{bmatrix} = \mathbf{D}(\tau) \begin{bmatrix} \Delta\boldsymbol{\theta}_k - \Delta\boldsymbol{\theta}_{SE} \\ \boldsymbol{\Omega}_k \end{bmatrix} + \begin{bmatrix} \Delta\boldsymbol{\theta}_{SE} \\ 0 \end{bmatrix}. \tag{73}$$

[In the case of the walking wheel, this set reduces to (56–59).] Define

$$\boldsymbol{\lambda} \equiv \begin{bmatrix} -1 \\ 1 \end{bmatrix}. \tag{74}$$

Then $\Delta\boldsymbol{\theta} = \boldsymbol{\lambda}\alpha_k$ at the start of the k-th stride, and $\Delta\boldsymbol{\theta} = -\boldsymbol{\lambda}\alpha_{k+1}$ at the end; hence, τ_k and α_{k+1} satisfy

$$-\boldsymbol{\lambda}\alpha_{k+1} = \mathbf{D}_{\theta\theta}(\tau_k)[\boldsymbol{\lambda}\alpha_k - \Delta\boldsymbol{\theta}_{SE}] + \mathbf{D}_{\theta\Omega}(\tau_k)\boldsymbol{\Omega}_k + \Delta\boldsymbol{\theta}_{SE} \tag{75}$$

where the submatrices $\mathbf{D}_{\theta\theta}$ and $\mathbf{D}_{\theta\Omega}$ form the top half of $\mathbf{D}$.

8. Support Transfer

When the forward leg strikes the ground, the impact is perfectly inelastic, some energy is dissipated, and support is transferred instantaneously. If the model has a torso, then an impulsive torque must be applied against the post-transfer stance leg to hold the torso in place. Also, an impulsive push $\boldsymbol{P}_{k+1}$ can be applied to pump the motion. The speed change produced by this combination of events satisfies

$$\boldsymbol{\Omega}_{k+1} = \boldsymbol{\Lambda}\boldsymbol{\Omega}(\tau_k) + \boldsymbol{\Gamma}\boldsymbol{P}_{k+1} \tag{76}$$

where $\boldsymbol{\Lambda}$ and $\boldsymbol{\Gamma}$ are derived in Appendix E. This is analogous to (29) for the rimless wheel: the first term accounts for angular momentum conservation at support transfer, and the second for the change in angular momentum produced by the impulse. Note that since the stance and swing legs exchange roles at support transfer, the leg indexing (71) must reverse between $\boldsymbol{\Omega}(\tau_k)$ and $\boldsymbol{\Omega}_{k+1}$. $\boldsymbol{\Lambda}$ (E.19) is defined to take care of the reordering.

Despite the complication introduced by the extra degree of freedom, the same effects that influence efficiency of support transfer in a rimless wheel also apply in a biped. In particular, high inertia and small α (16) are desirable. In the case of a biped, the effective "α" can be reduced by reducing stride length, increasing foot radius (as in the walking wheel) or raising the model's overall mass center (McGeer, 1990*b*).

Combining (76) with the transition eqns (73) and (75) produces the stride function

$$\begin{bmatrix} -\boldsymbol{\lambda}\alpha_{k-1} \\ \boldsymbol{\Omega}_{k+1} \end{bmatrix} = \begin{bmatrix} \mathbf{D}_{\theta\theta} & \mathbf{D}_{\theta\Omega} \\ \boldsymbol{\Lambda}\mathbf{D}_{\Omega\theta} & \boldsymbol{\Lambda}\mathbf{D}_{\Omega\Omega} \end{bmatrix} \begin{bmatrix} \boldsymbol{\lambda}\alpha_k - \Delta\boldsymbol{\theta}_{SE} \\ \boldsymbol{\Omega}_k \end{bmatrix} + \begin{bmatrix} \Delta\boldsymbol{\theta}_{SE} \\ \boldsymbol{\Gamma}\boldsymbol{P}_{k+1} \end{bmatrix}. \tag{77}$$

There are three initial conditions for each stride ($\alpha, \Omega_C, \Omega_F$), but four equations since τ_k must be found simultaneously [as in (60–63)].

9. Cyclic Walking Conditions

We now apply the cyclic-gait condition (2), and solve for τ_0, α_0, and $\boldsymbol{\Omega}_0$. First, solve for $\boldsymbol{\Omega}_0$ using the "$\boldsymbol{\Omega}$" equations of the stride function (77). Thus

$$\boldsymbol{\Omega}_0 = [\mathbf{I} - \Lambda \mathbf{D}_{\Omega\Omega}]^{-1}(\Lambda \mathbf{D}_{\Omega\theta}[\lambda\alpha_0 - \Delta\boldsymbol{\theta}_{SE}] + \Gamma \boldsymbol{P}_0). \tag{78}$$

Now define

$$\mathbf{D}'(\alpha_0, \tau_0) = \mathbf{D}_{\theta\theta} + \mathbf{D}_{\theta\Omega}[\mathbf{I} - \Lambda \mathbf{D}_{\Omega\Omega}]^{-1} \Lambda \mathbf{D}_{\Omega\theta}. \tag{79}$$

Then eliminating $\boldsymbol{\Omega}_0$ in the "$\boldsymbol{\theta}$" equations of the stride function leaves as the steady walking conditions

$$\boldsymbol{0} = [\mathbf{I} + \mathbf{D}']\lambda\alpha_0 + [\mathbf{I} - \mathbf{D}']\Delta\boldsymbol{\theta}_{SE} + \mathbf{D}_{\theta\Omega}[\mathbf{I} - \Lambda \mathbf{D}_{\Omega\Omega}]^{-1} \Gamma \boldsymbol{P}_0. \tag{80}$$

Consider first gravity-powered walking, with $\boldsymbol{P}_0 = \boldsymbol{0}$. The slope γ necessary to sustain the walk enters through $\Delta\boldsymbol{\theta}_{SE}$, which can be expressed as

$$\Delta\boldsymbol{\theta}_{SE} = \Delta\boldsymbol{\theta}_w + \boldsymbol{b}\gamma \tag{81}$$

where $\boldsymbol{b}$ accounts for the leaning necessary to balance on a slope, and $\Delta\boldsymbol{\theta}_w$ for any model asymmetry which would produce a non-vertical equilibrium on level ground. Putting (81) into the steady-gait condition (80), and setting $\boldsymbol{P}_0 = \boldsymbol{0}$, leaves

$$\boldsymbol{0} = [\mathbf{I} + \mathbf{D}']\lambda\alpha_0 + [\mathbf{I} - \mathbf{D}'][\Delta\boldsymbol{\theta}_w + \boldsymbol{b}\gamma]. \tag{82}$$

One can choose γ and solve this pair of equations for α_0 and τ_0, with $\boldsymbol{\Omega}_0$ following from (78). Alternatively, one can choose α_0 and solve γ and τ_0; this is easier since the equations are linear in γ. In any case solutions come in pairs, as we found for the walking wheel. Figure 6 shows examples. In experiments, gravity-powered bipeds

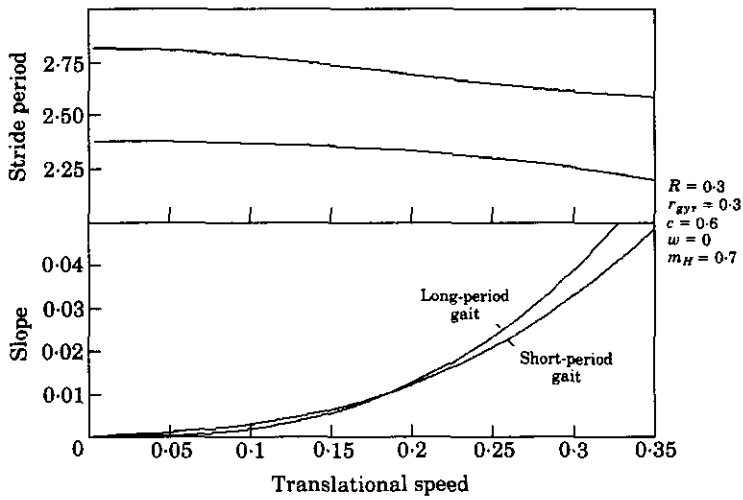

FIG. 6. Gravity-powered walking of an example straight-legged biped. Stride period τ_0 and slope γ_g are shown as functions of speed (in units of $\sqrt{gl}$). Model parameters are indicated on the right of the plot. (m_H is a point mass at the hip.) At any speed there are two possible cyclic gaits, which are distinguished by quite different periods. The short-period gait is unstable, so only long-period walking is sustainable under gravity power.

almost invariably adopt the longer-period gait (McGeer, 1990*b*, 1992). The shorter-period gait, meanwhile, seems to be unstable for all parameter choices, and is usually less efficient because the forward foot tends to strike with appreciable forward motion.

10. Energy Consumption in Steady Walking

Since gravity-powered walking has been discussed at length in the references, we wish to concentrate here upon powered walking. Toward this end let us develop a formula for energy consumption with toe-off impulses. As in the rimless wheel, the same momentum is transferred whether the impulses are applied pre- or post-support transfer, but in most cases the former strategy requires much less work. According to (31) it can be calculated from

$$W = \tfrac{1}{2}\boldsymbol{P}_{k+1}^T \boldsymbol{V}_p^+ \tag{83}$$

$\boldsymbol{V}_p^+$ being the post-impulse velocity of the original point of contact. Calculation of $\boldsymbol{V}_p^+$ proceeds by analogy with the derivation for the rimless wheel. Thus the impulse causes a momentary flight phase; translational and rotational velocities in this phase [cf. (23), (24) and (E.4)] are given by

$$\boldsymbol{V}_{CM_f} = \boldsymbol{V}_{CM}(\tau_k) + \boldsymbol{P}_{k+1} = \mathbf{G}\boldsymbol{\Omega}(\tau_k) + \boldsymbol{P}_{k+1} \tag{84}$$

$$\boldsymbol{\Omega}_f = \boldsymbol{\Omega}(\tau_k) - \mathbf{M}_f^{-1}\mathbf{G}^T\boldsymbol{P}_{k+1} \tag{85}$$

with $\mathbf{G}$ from (C.21) and $\mathbf{M}_f$ from (C.19). $\boldsymbol{V}_p^+$ [cf. (32)] is then

$$\boldsymbol{V}_p^+ = \boldsymbol{V}_{CM_f} - \mathbf{G}\boldsymbol{\Omega}_f = [\mathbf{I} + \mathbf{G}\mathbf{M}_f^{-1}\mathbf{G}^T]\boldsymbol{P}_{k+1}. \tag{86}$$

The work done by the impulse [cf. (35)] is therefore

$$W = \tfrac{1}{2}\boldsymbol{P}_{k+1}^T[\mathbf{I} + \mathbf{G}\mathbf{M}_f^{-1}\mathbf{G}^T]\boldsymbol{P}_{k+1}. \tag{87}$$

Notice that the energy input is quadratic in $\boldsymbol{P}_{k+1}$.

11. The Symmetric Impulse

We showed in section 4 that an impulse of just the right magnitude and direction (38) makes the rimless wheel free of dissipation when climbing slope $-\gamma_g$. Inspection of (80) suggests that the analogous "symmetric" impulse for a straight-legged biped is

$$\boldsymbol{P}_0 = [\mathbf{D}_{\theta\Omega}[\mathbf{I} - \boldsymbol{\Lambda}\mathbf{D}_{\Omega\Omega}]^{-1}\boldsymbol{\Gamma}]^{-1}[\mathbf{I} - \mathbf{D}']\boldsymbol{b}(\gamma_g - \gamma). \tag{88}$$

This eliminates γ from the cyclic-gait condition, so that the same (α_0, τ_0) which solve the system when $\boldsymbol{P}_0 = \boldsymbol{0}$ continue to hold regardless of slope. Figure 7 shows the work done by this impulse as a function of slope. The plot has the same format as in Fig. 4 for the rimless wheel, and all of the important features are common between the two plots.

If the impulse is not applied as specified by (88), then some penalty is incurred. Usually the penalty is not large, but if a particularly bad choice is made then the

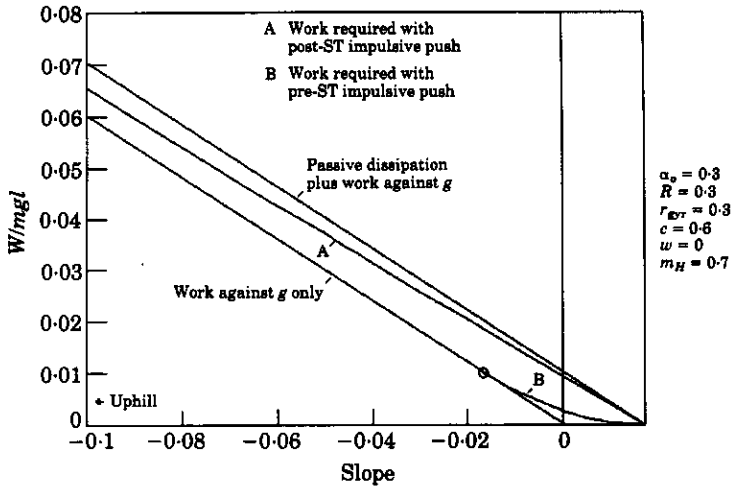

FIG. 7. Energy requirements for impulsive pumping of the biped walking cycle. Note the similarity to Fig. 4.

walking cycle can disappear. Figure 8 shows gait parameters (i.e. α_0 and τ_0) vs. impulse angle for a specified slope ($-0{\cdot}01$ rad) and speed ($0{\cdot}25\sqrt{gl}$). Also as an index of energy consumption it shows the *specific resistance*, defined as

$$SR = \frac{\text{energy dissipated}}{\text{weight} \times \text{distance traveled}}. \tag{89}$$

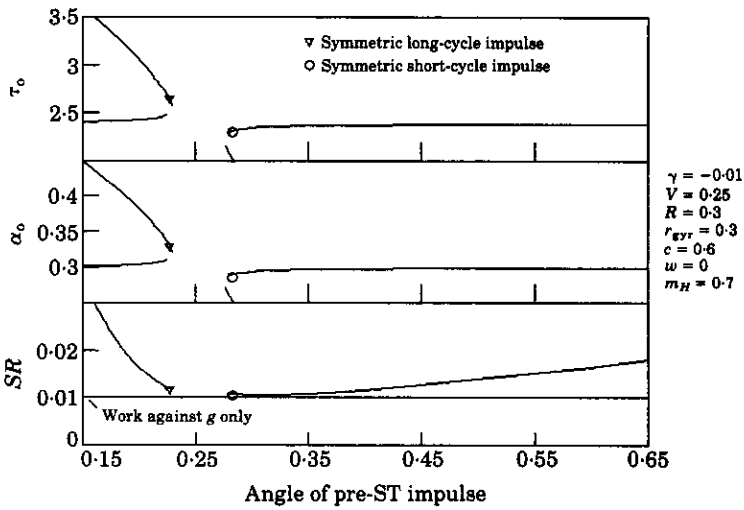

FIG. 8. Stride length, period, and "efficiency" as functions of the angle of a toe-off impulse. For each angle the impulse size is adjusted to maintain a speed of $0{\cdot}25\sqrt{gl}$ when climbing a 1% slope. Impulse angles between 0·23 and 0·28 rad should be avoided, since there turn out to be no cyclic gaits in this range (80). For any other angle, however, cyclic solutions come in pairs as in the gravity-powered case.

(Note that energy per step as in Fig. 7 would be a misleading indicator of efficiency, since in this plot is is *speed* that is being held constant rather than step length.) Starting at the left edge of the plot, with the impulse nearly vertical, one finds a choice between long- and short-period gaits. Then rotating the impulses forward brings the cyclic solutions together, until at a certain point they "pinch off". With further rotation they reappear and separate, but impulses between the pinch-off angles cannot sustain steady gaits. A review of the energy requirements over the remaining range of solutions indicates that the best strategy in this case would be to push at an angle of 0·3 rad or so; this would leave a prudent margin for error, while reducing energy consumption to a nearly optimal level. However the choice is not particularly critical, which is to say that walking has rather forgiving dynamics. All you have to do is push in more or less the right direction and your legs will take care of the rest.

12. Stability

Linearizing the stride function for the straight-legged biped (77) leads (as developed in the Appendix) to

$$\begin{bmatrix} \Delta\alpha_{k+1} \\ \Delta\boldsymbol{\Omega}_{k+1} \\ \Delta\tau_k \end{bmatrix} = \nabla_p \boldsymbol{S} \begin{bmatrix} \Delta\alpha_k \\ \Delta\boldsymbol{\Omega}_k \end{bmatrix} + \begin{bmatrix} \dfrac{\partial \boldsymbol{S}}{\partial P_x} & \dfrac{\partial \boldsymbol{S}}{\partial P_y} \end{bmatrix} \Delta \boldsymbol{P}_{k+1}. \tag{90}$$

There are four equations in the set, but only the first three are needed to assess stability. The fourth emerges as a bonus from the derivation, and allows one to solve for $\Delta\tau_k$. Thus the eigenvalues and eigenvectors listed in the example of Table 1 are those of the upper 3×3 submatrix of $\nabla_p \boldsymbol{S}$.

Figure 9 shows the modes of an example model, in the form of a root locus over a

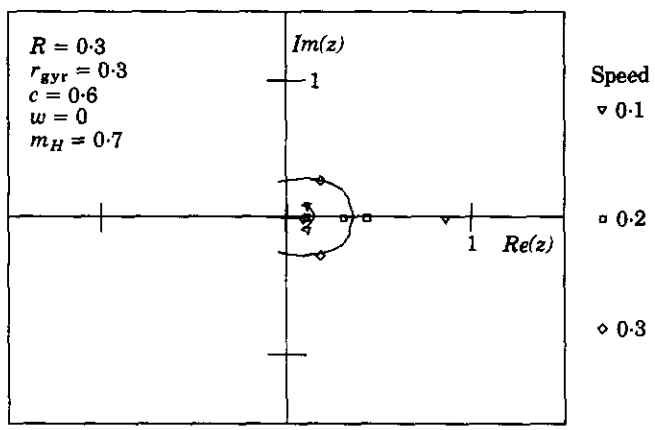

FIG. 9. Root locus for gravity-powered walking in the long-period gait. The three stride-to-stride eigenvalues for an example biped are plotted vs. speed. All loci remain within the unit circle, so gravity-powered walking is stable throughout the speed range. (However a similar locus for the short-period gait would show instability.)

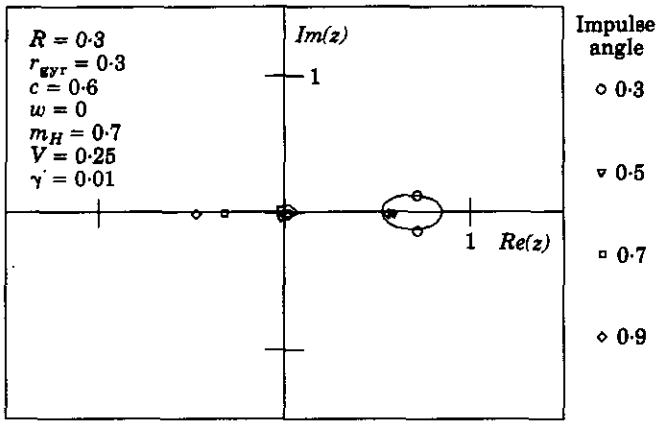

FIG. 10. Root locus vs. impulse angle. All three stride-to-stride eigenvalues remain stable over impulse angles ranging from 0·28 rad to more than 0·9 rad.

range of walking speeds. Here the modes are quite different from those in Table 1 (mainly because for this calculation we have specified a smaller foot radius). At low speed there is a well-defined "speed" mode, but the "totter" and "swing" modes merge into a conjugate pair. At high speed, on the other hand, the "swing" mode is distinct, but the "totter" and "speed" modes are coupled. In any event, the locus shows stability across the full speed range. However this conclusion applies only to the long-period set of gaits; the short-period set turns out to have a monotonic divergence in one mode.

Figure 9 was done for gravity-powered walking. Before doing similar calculations for impulse-powered walking, some thought must be given to mechanization of the impulse. We envision that a robot might use spring-loaded pistons in each foot. These would be cocked to a specified energy and, just before support transfer, fired in a specified direction. Hence the variables under direct control would be the impulsive work W and inclination ϕ_p (G.2). Appendix G explains how to linearize the stride function in terms of these variables; the result is

$$\begin{bmatrix} \Delta\alpha_{k+1} \\ \Delta\boldsymbol{\Omega}_{k+1} \\ \Delta\tau_k \end{bmatrix} = \nabla_W \boldsymbol{S} \begin{bmatrix} \Delta\alpha_k \\ \Delta\boldsymbol{\Omega}_k \end{bmatrix} + \frac{\partial \boldsymbol{S}}{\partial W} \Delta W_{k+1} + \frac{\partial \boldsymbol{S}}{\partial \phi_p} \Delta\phi_{p_{k+1}}. \tag{91}$$

If the impulsive work is kept constant from one stride to the next, then stability is indicated by the upper 3×3 submatrix of $\nabla_W \boldsymbol{S}$. An example is given in Fig. 10, which shows a root locus for the long-period gaits of Fig. 8. The locus shows that almost any impulse angle is acceptable as far as stability is concerned.

Similar analyses can be done to investigate sensitivity to each parameter of the model. Further examples are provided in McGeer (1990*a*, *b*). In general, passive locomotion proves to be quite robust with respect to parameter variations. Furthermore, stability can be augmented by feedback; possibilities are discussed in section 14.

13. Torso Orientation

The strategy of pushing with the trailing foot suffers from the obvious limitation that it only works for walking "uphill", i.e. for slopes above γ_g. To walk downhill length cycling can be used instead, as in the rimless wheel, but for a biped with a torso another option arises. In order to hold the torso motionless during the stride, a torque must be applied by reaction against the stance leg. This torque is derived in the Appendix (D.22); the reaction against the stance leg is

$$T_{C/T} = -I_{TC}\dot{\Omega}_C + m_T c_T(\theta_T + \gamma). \tag{92}$$

Thus holding the torso in a backward recline brakes the stance leg, and so dissipates energy into whatever device is applying the torque. (In animals this means heat generation in muscle, but a robot might make provision for regenerative braking.) On the other hand, leaning the torso forward allows the stance/torso actuator to pump energy into walking and so supplement the impulsive push.

In any case, the energy transferred over one stride is

$$W_H = \int_{-\alpha_0}^{\alpha_0} T_{C/T}\,\mathrm{d}\theta_C = \frac{I_{TC}}{2}(\Omega_{C_0}^2 - \Omega_C^2(\tau_0)) + 2m_T c_T(\theta_T + \gamma)\alpha_0. \tag{93}$$

For shallow slopes $\Omega_{C_0} \approx \Omega_C(\tau_0)$; making this approximation and matching actuator work to the potential energy change per stride (37) leaves

$$\theta_T + \gamma \approx \frac{-1}{m_T c_T}(\gamma - \gamma_g). \tag{94}$$

With $m_T = 0{\cdot}7$ and $c_T = 0{\cdot}3$, for example, the required torso recline (from the vertical) works out to about 4·8 rad per radian of slope if no other method is used to dissipate energy.

To check this result against an exact calculation, we return to the stride function (77). The torso angle enters through $\Delta\boldsymbol{\theta}_{SE}$ (81), which can be written as

$$\Delta\boldsymbol{\theta}_{SE} = \Delta\boldsymbol{\theta}_w|_{\theta_T=0} + \boldsymbol{a}_T\theta_T + \boldsymbol{b}_T\gamma \tag{95}$$

with $\boldsymbol{a}_T$ from (D.25). To find a steady walk with a leaning torso, we simply choose a desired θ_T and solve for the cyclic-gait [eqn (80)]. Figure 11 shows a range of example results. The relationship between torso angle and slope proves to be as predicted by (94), and—at least for the long-period gait—the stride period varies in the intuitive sense: a braking torque on the stance leg slows the cadence, and a thrusting torque accelerates the cadence. But accelerated cadence causes a problem: at $(\theta_T + \gamma) = 0{\cdot}045$ (in this example) the long- and short-period solutions "pinch-off" and disappear. The model cannot walk with the torso leaning further forward.

This is no great restriction, since one has no particular need to walk and bow at the same time; however, in any case, the restriction is easily removed. As Fig. 11 indicates, a small offset of the legs' mass centers (w) shifts the pinch-off θ_T substantially. Pinch-off still occurs at the same τ_0 (satisfying $\omega_F\tau_0 \approx \pi$), but not at the same γ. Humans may exploit this effect. When leaning forward we walk on the balls of the

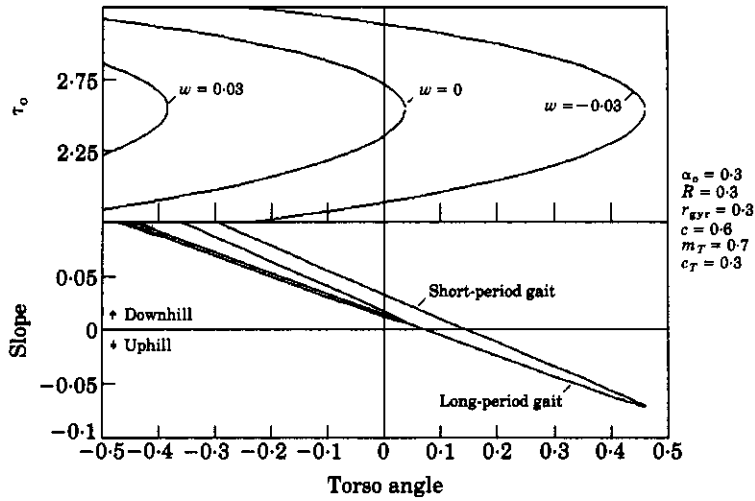

FIG. 11. Gait adjustment by torso inclination. The torso can be held in a backward recline by applying a torque against the stance leg. The reaction brakes the leg, and so allows a steep descent. Conversely, the torso can be inclined forward for climb. However, the dynamics of the model are not symmetric; leaning forward too far makes the cyclic solutions disappear. Fortunately, the vanishing point can be adjusted by making w (Fig. 5) non-zero.

feet, which effectively shifts the leg axes forward with respect to the mass centers, and so makes w negative just as required by Fig. 11.

w in fact proves to be something of a panacea. It can also be used to compensate for friction in the joints, which otherwise would be intolerable (McGeer, 1990*b*), and generally in any other situation when τ_0 has to be shifted into a more acceptable range. McGeer (1990*a*, *c*) offers more examples.

14. Scattered Stepping Stones

To this point we have concentrated on steady walking over uniform terrain. However one also must be able to negotiate more difficult situations, and as an elementary example consider the *stepping stone* problem. A one-dimensional field of stepping stones is randomly spaced along the model's path. The problem is to modulate the gait from stride to stride such that the feet land on top of each stone.

We take up the issue at the start of the k-th stride. By some means, visual or otherwise, we measure the distance to the next stepping stone; this determines the desired value for α_{k+1}. Thus, in terms of the stride function (77), the left-hand side of the two "$\boldsymbol{\theta}$" equations is specified. The control problem is to adjust two parameters on the right-hand side so that the two equations are satisfied.

The most convenient parameters mathematically are the two elements of $\Delta\boldsymbol{\theta}_{SE}$, since these allow a linear solution. Thus, solving (77) for a suitable value of $\Delta\boldsymbol{\theta}_{SE}$ leaves

$$\Delta\boldsymbol{\theta}_{SE_k} = [\mathbf{D}_{\theta\theta} - \mathbf{I}]^{-1}(\boldsymbol{\lambda}\alpha_{k+1} + \mathbf{D}_{\theta\theta}\boldsymbol{\lambda}\alpha_k + \mathbf{D}_{\theta\Omega}\boldsymbol{\Omega}_k). \tag{96}$$

Once τ_k is chosen (to fix $\mathbf{D}$), $\Delta\boldsymbol{\theta}_{SE_k}$ follows. It, in turn, can be set via torques applied between the torso and each leg. Thus, the required torques, from (D.4) and (D.17), are

$$\begin{bmatrix} T_C \\ T_F \end{bmatrix}_k = \mathbf{K}(\Delta\boldsymbol{\theta}_{SE_k} - \Delta\boldsymbol{\theta}_w - \boldsymbol{b}\gamma). \tag{97}$$

Note that these remain constant throughout the stride.

The big problem with this scheme is that the torque applied to the torso, namely $-(T_C+T_F)$, is, in general, *not* the torque required to hold the torso at its original angle (92). The obvious solution might appear to be rotation of the torso to a suitable new angle; however, this turns out not to work. Suppose, for example, that a long stride were required; this would call for a positive torque on the stance leg, and so a positive θ_T. But rotating the torso forward *dynamically* causes the stance leg to recoil backward, which produces an effect exactly opposite to that desired! Dynamic adjustment of torso angle is therefore not very helpful.

Alternatively, then, we might discard $\Delta\boldsymbol{\theta}_{SE_k}$ as the stepping-stone control and instead adjust $\boldsymbol{P}_k$. For this purpose the "$\boldsymbol{\theta}$" equations of the stride function can be written as

$$-\lambda\alpha_{k+1} = \mathbf{D}_{\theta\theta}(\lambda\alpha_k - \Delta\boldsymbol{\theta}_{SE_k}) + \mathbf{D}_{\theta\Omega}(\boldsymbol{\Lambda\Omega}(\tau_{k-1}) + \boldsymbol{\Gamma P}_k) + \Delta\boldsymbol{\theta}_{SE_k}. \tag{98}$$

Solving for $\boldsymbol{P}_k$ gives

$$\boldsymbol{P}_k = \boldsymbol{\Gamma}^{-1}\mathbf{D}_{\theta\Omega}^{-1}(-\lambda\alpha_{k+1} - \Delta\boldsymbol{\theta}_{SE_k} - \mathbf{D}_{\theta\theta}(\lambda\alpha_k - \Delta\boldsymbol{\theta}_{SE_k}) - \mathbf{D}_{\theta\Omega}\boldsymbol{\Lambda\Omega}(\tau_{k-1})). \tag{99}$$

Again, this control strategy is convenient mathematically. However it can run into trouble on short strides, which may call for a shallow impulse angle or even an inadmissible downward pull.

A third stepping-stone strategy which would avoid the shallow-angle problem uses one torque and one impulse variable as the control pair. In particular, the impulse angle could be specified *a priori*, leaving the magnitude as the first control variable. The second could be a stance/torso torque T_H added to $T_{C/T}$ from (92), and balanced by a swing/torso torque $-T_H$. Together these would leave the torso undisturbed. Meanwhile the stride function is linear in the two control variables, so again the appropriate values are easily calculated, and the solution easily implemented so long as $\boldsymbol{P}_k$ remains positive.

One final alternative is to use T_H as a single control variable, and vary τ_k as the second free parameter in solving the "$\boldsymbol{\theta}$" equations. Figure 12 shows an example of this technique. Unfortunately the stride function is non-linear in τ_k, and this introduces certain restrictions. First, it makes solution for T_H less convenient than in the previous schemes. More fundamentally, it means that in some cases there is simply no solution to be found. Large changes in stride length are particularly problematic.

Nevertheless this technique allows a quite useful range of gait modulation, as do the other methods which we have discussed. In combination they can achieve very dextrous locomotion. Moreover, their application is not just for the stepping-stone problem. They can be used simply as regulators to augment the stride-to-stride

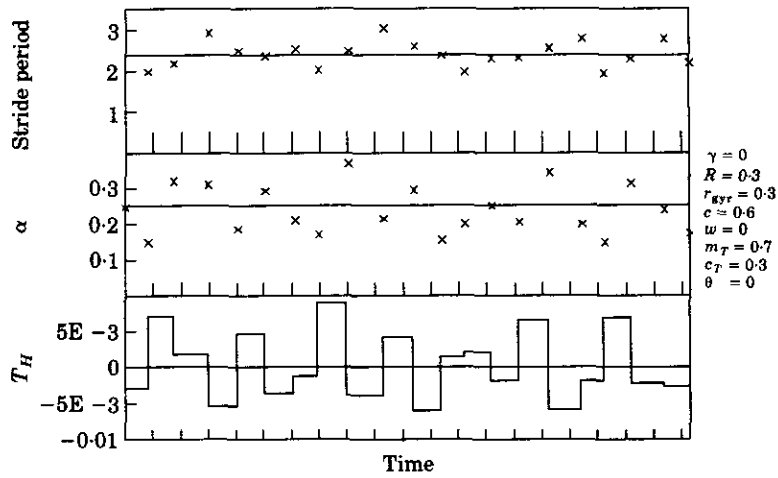

FIG. 12. Modulation of the walking cycle. A passive biped can walk across randomly scattered stepping stones by modulating its cycle from stride to stride. Here, the modulation is controlled by a torque T_H applied between the legs. Notice that the torque is selected at the start of each stride, and then held constant until the next heel strike.

stability of steady walking. In fact, the "T_H" technique can be applied at any time during the motion, and so can compensate for disturbances arising in midstride.

15. Free and Easy

It is sometimes assumed, by both students of biomechanics and designers of robotic analogs, that walking requires complex motor control. This is certainly not so. In fact if one is satisfied only to go downhill then walking can be completely free. If, on the other hand, one wants to go uphill or to negotiate uneven terrain, then walking, while not quite free, is still very easy; one need only pump and modulate the passive limit cycle. The forgiving dynamics at play allow a child easily to learn the necessary techniques (thankfully without benefit of our mathematical recapitulation!) and the locomotion repertoire that results offers an attractive combination of dexterity, efficiency, and simplicity. Engineers, of course, prefer to travel on wheels; however, for an organism fated to evolve in the absence of well-graded highways, legs are a natural alternative.

REFERENCES

ALEXANDER, R. M. (1988). *Elastic Mechanisms in Animal Movement*. Cambridge: Cambridge University Press.

MCGEER, T. (1988). *Stability and Control of Two-dimensional Biped Walking*. Technical Report CSS-IS TR 88-01. Burnaby, BC: Simon Fraser University Centre for Systems Science, September.

MCGEER, T. (1990*a*). Passive bipedal running. *Proc. R. Soc. B* **1240**, 107–134.

MCGEER, T. (1990*b*). Passive dynamic walking. *Intern. J. Robot Res.* **9(2)**, 68–82, April.

MCGEER, T. (1990*c*). Passive walking with knees. In: *Proc. 1990 IEEE Robotics & Automation Conference*, May 1990. Cincinnati, OH: pp. 1640–1645.

McGeer, T. (1991). Passive dynamic biped catalogue, 1991. In: *Proc. 2nd Int. Symp. of Experimental Robotics*, June (Chatila, R., ed.). New York: Springer-Verlag, in press.
McGeer, T. (1992). Principles of walking and running. In: *Advances in Comparative and Environmental Physiology*, Vol. 11, *Mechanics of Animal Locomotion* (Alexander, R. M., ed.). Berlin: Springer-Verlag.
McMahon, T. A. (1984). Mechanics of locomotion. *Intern. J. Robot. Res.* **3(2)**, 4–28.
Mochon, S. & McMahon, T. A. (1980). Ballastic walking: an improved model. *Math. Biosci.* **52**, 241–260.
Thompson, C. & Raibert, M. C. (1989). Passive dynamic running. In: *Proc. 1st Int. Symp. of Experimental Robotics* (Hayward, V. & Khatib, O., eds) pp. 74–83. New York: Springer-Verlag.

APPENDIX A

Sub- and Superscripts

$+$	immediately after support transfer	g	due to gravity
$-$	immediately before support transfer	H	at the hip
0	cycle-gait condition	h	at heel strike
a	start-of-stride	k	stride index
b	end-of-stride	p	impulse application point
C	stance leg	SE	static equilibrium
c	contact point	T	(as subscript) torso
CM	overall center of mass	T	(as superscript) matrix transpose
F	swing leg	x	normal to ground
f	flight phase	y	parallel to ground

APPENDIX B

Symbols

(Defining equations are noted in parentheses.)

Roman

a_T	derivative of static equilibrium *w.r.t.* torso angle (D.25)	E	energy (44)
b	derivative of static equilibrium *w.r.t.* slope (D.24)	$\mathbf{F}_T$	stance/swing index exchanger (E.2)
c	distance from foot to leg mass center (Fig. 5)	F_c	contact force (C.1)
$\mathbf{D}$	start- to end-of-stride transition matrix (F.4)	f	stride function error vector (F.1)
$\mathbf{D}_{\theta\theta}, \mathbf{D}_{\theta\Omega}, \mathbf{D}_{\Omega\theta}, \mathbf{D}_{\Omega\Omega}$	submatrices of start- to end-of-stride transition matrix	$\mathbf{G}$	CM velocity Jacobian (C.21), (D.2)
		g	gravitational acceleration (D.12)
$\mathbf{D}'$	(79)	H	angular momentum
		$\mathscr{H}$	angular impulse
		$\mathbf{I}$	identity matrix
		I	moment of inertia

$\mathbf{K}$ stance stiffness matrix (D.18)
l leg length (Fig. 5)
$\mathbf{M}$ stance inertia matrix (D.23)
$\mathbf{M}_0$ $\mathbf{M}$ for $\theta_C = 0$, $\theta_F = \pi$ (72)
$\mathbf{M}_f$ flight-phase inertia matrix (C.19)
m mass (Fig. 5)
$\boldsymbol{P}$ toe-off impulse
P magnitude of toe-off impulse (G.2)
$\boldsymbol{p}$ toe-off impulse of unit magnitude (G.2)
$\mathbf{Q}$ diagonal matrix of eigenvalues (F.3)
R foot radius (Fig. 5)
$\boldsymbol{r}$ position vector
r_{gyr} radius of gyration
S stride function (1)
∇S gradient of stride function (3)
SR specific resistance (89)
T torque
V linear velocity
W energy input (31), (47)
w offset from leg axis to leg mass center (Fig. 5)
$\hat{x}$ unit vector normal to ground
$\hat{y}$ unit vector parallel to ground
z eigenvalue of ∇S (6)

Greek

α leg angle at support transfer (74)
$\boldsymbol{\Gamma}$ impulse-coupling matrix (E.20), (76), (27)
γ slope (Fig. 5)
θ link angle
$\Delta\theta$ rotation from surface normal (Fig. 5)
$\Delta\theta_{SE}$ static equilibrium position (81), (95)
$\Delta\theta_w$ static equilibrium on level ground (D.19)
η coefficient of restitution (16)
$\boldsymbol{\Lambda}$ support transfer matrix (E.19), (76)
λ (74)
$\boldsymbol{\nu}$ start-of-stride state vector (1)
σ rimless wheel timescale parameter (8)
τ dimensionless time $t\sqrt{g/l}$
$\boldsymbol{\Phi}$ matrix of eigenvectors (F.3)
ϕ_p angle of $\boldsymbol{p}$ *w.r.t.* trailing leg (G.2)
Ω angular speed
ω_F swing pendulum frequency

APPENDIX C

General Equations of Motion

We now derive the equations of motion for the biped of Fig. 5. Translation of the overall mass center is governed by

$$\boldsymbol{V}_{CM} = \boldsymbol{g} + \boldsymbol{F}_c \tag{C.1}$$

where $\boldsymbol{F}_c$ is the force at the point of contact, normalized by total mass. (Also note that $g = 1$ in normalized units.) Meanwhile rotation of each link is governed by an equation of the form

$$\frac{dH}{dt} = T \tag{C.2}$$

where H is the angular momentum and T the torque about the hip. Formulation of this equation proceeds similarly for each link. Consider the stance leg. The left-hand

side is

$$\frac{dH_C}{dt} = m_{leg}(r_{gyr}^2 \dot{\Omega}_C + r_{HC} \times \dot{V}_C) \tag{C.3}$$

r_{HC} is the vector from the hip to leg mass center, and $\dot{V}_C$ the acceleration at the mass center. $\dot{V}_C$ can be separated into components due to translation and rotation. The translational component is just $\dot{V}_{CM}$. The rotational component is derived as follows. First, call $r_{CM/C}$ the vector from overall mass center to leg mass center. This is

$$r_{CM/C} = r_{HC} - r_{H/CM}. \tag{C.4}$$

The vector from hip to overall mass center is, in turn,

$$r_{H/CM} = m_{leg}(r_{HC} + r_{HF}) + m_T r_{HT} \tag{C.5}$$

where m_{leg} and m_T are normalized by total mass. Thus from (C.4)

$$r_{CM/C} = (1 - m_{leg}) r_{HC} - m_{leg} r_{HF} - m_T r_{HT}. \tag{C.6}$$

Differentiating for velocity gives

$$\frac{dr_{CM/C}}{dt} = (1 - m_{leg}) \Omega_C \times r_{HC} - m_{leg} \Omega_F \times r_{HF} - m_T \Omega_T \times r_{HT} \tag{C.7}$$

where the Ω vector points into the page in Fig. 5. Differentiating again leaves the component of $\dot{V}_C$ due to rotation about the overall mass center:

$$\begin{aligned} \frac{d^2 r_{CM/C}}{dt^2} = & -(1 - m_{leg}) r_{HC} \Omega_C^2 + m_{leg} r_{HF} \Omega_F^2 + m_T r_{HT} \Omega_T^2 \\ & + (1 - m_{leg}) \dot{\Omega}_C \times r_{HC} - m_{leg} \dot{\Omega}_F \times r_{HF} - m_T \dot{\Omega}_T \times r_{HT}. \end{aligned} \tag{C.8}$$

Substituting this into the formula for H_C (C.3) completes the left-hand side of the rotational equation for the stance leg (C.2):

$$\begin{aligned} \frac{dH_C}{dt} = & m_{leg}(r_{gyr}^2 + (1 - m_{leg}) |r_{HC}|^2) \dot{\Omega}_C \\ & - m_{leg}^2 r_{HC} \cdot r_{HF} \dot{\Omega}_F - m_{leg} m_T r_{HC} \cdot r_{HT} \dot{\Omega}_T \\ & + m_{leg}^2 r_{HC} \times r_{HF} \Omega_F^2 + m_{leg} m_T r_{HC} \times r_{HT} \Omega_T^2 + m_{leg} r_{HC} \times \dot{V}_{CM}. \end{aligned} \tag{C.9}$$

Now turn attention to the torques on the right-hand side of (C.2). Components are due to gravity, the contact force, and a control torque at the hip. The gravitational component is

$$T_{C_g} = m_{leg} r_{HC} \times g. \tag{C.10}$$

The component due to the contact force, from (C.1), is

$$T_{F_c} = -r_{cH} \times F_c = -r_{cH} \times (\dot{V}_{CM} - g) \tag{C.11}$$

where r_{cH} is the vector from contact point to hip. Adding these two components together with a control torque T_C gives

$$T_{C_f} = (r_{cH} + m_{leg} r_{HC}) \times g - r_{cH} \times \dot{V}_{CM} + T_C. \tag{C.12}$$

Combining this result with the angular momentum (C.9) completes the rotational equation of motion (C.2) for the stance leg. Similar derivations follow for the swing leg and torso; the three equations together have the form

$$\mathbf{M}_{T_f}\dot{\boldsymbol{\Omega}}+\mathbf{C}_f\boldsymbol{\Omega}^2=\mathbf{G}^T(g-\dot{V}_{CM})+T. \tag{C.13}$$

The matrices are as follows. Define

$$I_{L_f}\equiv m_{\text{leg}}(r_{\text{gyr}}^2+(1-m_{\text{leg}})|r_{HC}|^2) \tag{C.14}$$

$$I_{T_f}\equiv m_T(r_{\text{gyr}_T}^2+(1-m_T)c_T^2) \tag{C.15}$$

$$I_{FC_f}\equiv -m_{\text{leg}}^2 r_{HC}\cdot r_{HF} \tag{C.16}$$

$$I_{TC_f}\equiv -m_{\text{leg}}m_T r_{HC}\cdot r_{HT} \tag{C.17}$$

$$I_{TF_f}\equiv -m_{\text{leg}}m_T r_{HF}\cdot r_{HT}. \tag{C.18}$$

Then

$$\mathbf{M}_{T_f}=\begin{bmatrix} I_{L_f} & I_{FC_f} & I_{TC_f} \\ I_{FC_f} & I_{L_f} & I_{TF_f} \\ I_{TC_f} & I_{TF_f} & I_{T_f} \end{bmatrix} \tag{C.19}$$

$$\mathbf{C}_f=\begin{bmatrix} 0 & m_{\text{leg}}^2 r_{HC}\times r_{HF} & m_T m_{\text{leg}} r_{HC}\times r_{HT} \\ m_{\text{leg}}^2 r_{HF}\times r_{HC} & 0 & m_T m_{\text{leg}} r_{HF}\times r_{HT} \\ m_T m_{\text{leg}} r_{HT}\times r_{HC} & m_T m_{\text{leg}} r_{HT}\times r_{HF} & 0 \end{bmatrix} \tag{C.20}$$

$$\mathbf{G}=\begin{bmatrix} -\hat{y} \\ \hat{x} \end{bmatrix}\odot\begin{bmatrix} (r_{cH}+m_{\text{leg}}r_{HC}) & m_{\text{leg}}r_{HF} & m_T r_{HT} \end{bmatrix} \tag{C.21}$$

where $\odot$ indicates a dot product in each element of the matrix multiplication.

APPENDIX D

Stance Dynamics

The rotational eqn (C.13) applies regardless of whether the model is off the ground or in contact. When off the ground, $\dot{V}_{CM}=g$. When in contact, on the other hand, $\dot{V}_{CM}$ is determined by $\dot{\boldsymbol{\Omega}}$ as follows. Take the origin of co-ordinates to be the contact point at midstance. Then from (C.5) the position of the overall mass center is

$$\begin{aligned} r_{O/CM} &= \hat{y}R\theta_C+r_{cH}+r_{H/CM} \\ &= \hat{y}R\theta_C+r_{cH}+m_{\text{leg}}(r_{HC}+r_{HF})+m_T r_{HT}. \end{aligned} \tag{D.1}$$

Differentiating this [from (C.21)] gives

$$V_{CM}=\mathbf{G}\boldsymbol{\Omega} \tag{D.2}$$

where $\mathbf{G}$ is as in (C.13). Differentiating again gives the acceleration,

$$\dot{V}_{CM}=\mathbf{G}\dot{\boldsymbol{\Omega}}+\begin{bmatrix} -\hat{y} \\ \hat{x} \end{bmatrix}\odot\begin{bmatrix} \dfrac{\mathrm{d}(r_{cH}+m_{\text{leg}}r_{HC})}{\mathrm{d}\theta_C} & m_{\text{leg}}\dfrac{\mathrm{d}r_{HF}}{\mathrm{d}\theta_F} & m_T\dfrac{\mathrm{d}r_{HT}}{\mathrm{d}\theta_T} \end{bmatrix}\boldsymbol{\Omega}^2. \tag{D.3}$$

Substituting into (C.13) produces the stance-phase equations

$$\mathbf{M}_T\dot{\boldsymbol{\Omega}}+\mathbf{C}\boldsymbol{\Omega}^2=\mathbf{G}^T\boldsymbol{g}+\boldsymbol{T} \tag{D.4}$$

where the new matrices are as follows. Define

$$I_C \equiv m_{\text{leg}}(r_{\text{gyr}}^2+|\boldsymbol{r}_{cH}+\boldsymbol{r}_{HC}|^2)+(1-m_{\text{leg}})|\boldsymbol{r}_{cH}|^2 \tag{D.5}$$

$$I_F \equiv m_{\text{leg}}(r_{\text{gyr}}^2+|\boldsymbol{r}_{HF}|^2) \tag{D.6}$$

$$I_T \equiv m_{\text{leg}}(r_{\text{gyr}}^2+c_T^2) \tag{D.7}$$

$$I_{FC} \equiv m_{\text{leg}}\boldsymbol{r}_{HF}\cdot\boldsymbol{r}_{cH} \tag{D.8}$$

$$I_{TC} \equiv m_T\boldsymbol{r}_{HT}\cdot\boldsymbol{r}_{cH}. \tag{D.9}$$

Then

$$\mathbf{M}_T=\mathbf{M}_{T_f}+\mathbf{G}^T\mathbf{G}=\begin{bmatrix} I_C & I_{FC} & I_{TC} \\ I_{FC} & I_F & 0 \\ \mathrm{I_{TC}} & 0 & \mathrm{I_T} \end{bmatrix} \tag{D.10}$$

$$\mathbf{C}=\begin{bmatrix} -R(\boldsymbol{r}_{cH}+m_{\text{leg}}\boldsymbol{r}_{HC})\cdot\hat{y} & m_{\text{leg}}\boldsymbol{r}_{HF}\times\boldsymbol{r}_{cH} & m_T\boldsymbol{r}_{HT}\times\boldsymbol{r}_{cH} \\ -m_{\text{leg}}(\boldsymbol{r}_{HF}\times\boldsymbol{r}_{cH}+R\boldsymbol{r}_{HF}\cdot\hat{y}) & 0 & 0 \\ -m_T(\boldsymbol{r}_{HT}\times\boldsymbol{r}_{cH}+R\boldsymbol{r}_{HT}\cdot\hat{y}) & 0 & 0 \end{bmatrix}. \tag{D.11}$$

The $(\hat{x}, \hat{y})$ components of the vectors in these equations are

$$\boldsymbol{g}=\begin{bmatrix} -\cos\gamma \\ \sin\gamma \end{bmatrix} \tag{D.12}$$

$$\boldsymbol{r}_{HC}=(l-c)\begin{bmatrix} -\cos\theta_C \\ -\sin\theta_C \end{bmatrix}+w\begin{bmatrix} -\sin\theta_C \\ \cos\theta_C \end{bmatrix} \tag{D.13}$$

$$\boldsymbol{r}_{HF}=(l-c)\begin{bmatrix} \cos\theta_F \\ \sin\theta_F \end{bmatrix}+w\begin{bmatrix} \sin\theta_F \\ -\cos\theta_F \end{bmatrix} \tag{D.14}$$

$$\boldsymbol{r}_{HT}=c_T\begin{bmatrix} \cos\theta_T \\ \sin\theta_C \end{bmatrix} \tag{D.15}$$

$$\boldsymbol{r}_{cH}=\begin{bmatrix} R \\ 0 \end{bmatrix}+(l-R)\begin{bmatrix} \cos\theta_C \\ \sin\theta_C \end{bmatrix}. \tag{D.16}$$

In walking, rotations remain small, so the equations of motion (D.4) can be linearized. Thus the centrifugal ($\boldsymbol{\Omega}^2$) terms are dropped, $\mathbf{M}_T$ is evaluated at $\theta_C=0$, $\theta_F=\pi$, and the gravitational terms become

$$\mathbf{G}^T\boldsymbol{g}\approx\mathbf{K}_T[\Delta\boldsymbol{\theta}_{wT}+\boldsymbol{b}_T\gamma-\Delta\boldsymbol{\theta}] \tag{D.17}$$

where

$$\mathbf{K}_T\equiv g\begin{bmatrix} m_{\text{leg}}(c-R+ \\ (m_{\text{leg}}+m_T)(l-R) & 0 & 0 \\ 0 & -m_{\text{leg}}(l-c) & 0 \\ 0 & 0 & m_Tc_T \end{bmatrix} \tag{D.18}$$

$$\Delta\boldsymbol{\theta}_{wT} \equiv g\mathbf{K}_T^{-1}\begin{bmatrix} m_{\text{leg}}\, w \\ m_{\text{leg}}\, w \\ 0 \end{bmatrix} \tag{D.19}$$

$$\boldsymbol{b}_T \equiv g\mathbf{K}_T^{-1}\begin{bmatrix} m_{\text{leg}}c+(m_{\text{leg}}+m_T)l \\ -m_{\text{leg}}(l-c) \\ m_T c_T \end{bmatrix}. \tag{D.20}$$

The equations of motion (D.4) thus reduce to

$$\mathbf{M}_{T_0}\dot{\boldsymbol{\Omega}}+\mathbf{K}_T\Delta\boldsymbol{\theta} = \mathbf{K}_T[\Delta\boldsymbol{\theta}_{wT}+\boldsymbol{b}_T\gamma]+\boldsymbol{T}. \tag{D.21}$$

Now we wish to hold the torso motionless while the stride proceeds, which means that we must choose T_T (the third element of T) such that $\dot{\Omega}_T = 0$ throughout. Solving the third equation in this set for T_T thus leaves

$$T_T = I_{TC}\dot{\Omega}_C - m_T c_T g(\theta_T+\gamma). \tag{D.22}$$

This torque is to be applied by reaction against the stance leg; hence $-T_T$ must be added to the first equation. The equations for θ_C and θ_F are then left as quoted in (72) and (95), with $\mathbf{K}$ being the upper 2×2 submatrix of $\mathbf{K}_T$, $\Delta\boldsymbol{\theta}_w$ the first two elements of $\Delta\boldsymbol{\theta}_{wT}$, and the remaining terms as follows:

$$\mathbf{M} \equiv \begin{bmatrix} I_C+I_{TC} & I_{FC} \\ I_{FC} & I_F \end{bmatrix} \tag{D.23}$$

$$\boldsymbol{b} \equiv g\mathbf{K}^{-1}\begin{bmatrix} m_{\text{leg}}(l+c)+m_T(l+c_T) \\ -m_{\text{leg}}(l-c) \end{bmatrix} \tag{D.24}$$

$$\boldsymbol{a}_T \equiv g\mathbf{K}^{-1}\begin{bmatrix} m_T c_T \\ 0 \end{bmatrix}. \tag{D.25}$$

APPENDIX E

Support Transfer and Impulse Coupling

Calculation of impulse coupling and support transfer for a straight-legged biped proceeds by analogy with the rimless wheel case (23–28). Some care must be applied to maintain consistent leg indexing. In this derivation we will use the following convention: $\mathbf{G}^-$ and $\mathbf{G}^+$ will indicate values of $\mathbf{G}$ calculated according to (C.21), respectively, using *pre-* and *post*-ST indexing of $\boldsymbol{\theta}$—i.e. in evaluating (C.21) for $\mathbf{G}^-$, θ_C refers to the angle of the trailing leg; for $\mathbf{G}^+$, θ_C refers to the angle of the leading leg. $\boldsymbol{\Omega}$ will be ordered throughout according to the *post*-ST indexing, i.e. leading leg first.

If the impulse is applied prior to support transfer, then direct integration of (C.13) gives the instantaneous change in $\boldsymbol{\Omega}$. With *post*-ST indexing of $\boldsymbol{\Omega}$, the result is

$$\mathbf{F}_T\mathbf{M}_{T_f}^{-}\mathbf{F}_T(\boldsymbol{\Omega}_f-\boldsymbol{\Omega}^-) = -\mathbf{F}_T\mathbf{G}^{-T}\boldsymbol{P} \tag{E.1}$$

where $\mathbf{F}_T$ is the index-exchanging matrix

$$\mathbf{F}_T \equiv \begin{bmatrix} 0 & 1 & 0 \\ 1 & 0 & 0 \\ 0 & 0 & 1 \end{bmatrix}. \tag{E.2}$$

But

$$\mathbf{F}_T \mathbf{M}_{T_f}^- \mathbf{F}_T = \mathbf{M}_{T_f}^+ \tag{E.3}$$

where $\mathbf{M}_{T_f}^+$ is evaluated from (C.19) with *post*-ST link angles. Thus, solving (E.1) for the flight-phase $\boldsymbol{\Omega}$ gives [cf. (24), (85)]

$$\boldsymbol{\Omega}_f = \boldsymbol{\Omega}^- - \mathbf{M}_{T_f}^{+-1} \mathbf{F}_T \mathbf{G}^{-T} \boldsymbol{P}. \tag{E.4}$$

Provided that the forward foot continues to translate downward after the impulse, the flight phase ends immediately. The landing generates a second impulse $\boldsymbol{P}_h$, and we also apply a torsional impulse $\mathscr{H}$ to null torso rotation. Integrating the equations of motion through these events gives [cf. (26)]

$$\mathbf{M}_{T_f}^+ \boldsymbol{\Omega}^+ = \mathbf{M}_{T_f}^+ \boldsymbol{\Omega}_f - \mathbf{G}^{+T} \boldsymbol{P}_h + \mathscr{H}. \tag{E.5}$$

$\boldsymbol{P}_h$ [cf. (25)] is

$$\boldsymbol{P}_h = \boldsymbol{V}_{CM}^+ - \boldsymbol{V}_{CM_f} = \mathbf{G}^+ \boldsymbol{\Omega}^+ - (\mathbf{G}^- \mathbf{F}_T \boldsymbol{\Omega}^- + \boldsymbol{P}). \tag{E.6}$$

Substituting this and (E.4) into (E.5) leaves

$$[\mathbf{M}_{T_f}^+ + \mathbf{G}^{+T} \mathbf{G}^+] \boldsymbol{\Omega}^+ = [\mathbf{M}_{T_f}^+ + \mathbf{G}^{+T} \mathbf{G}^- \mathbf{F}_T] \boldsymbol{\Omega}^- + [\mathbf{G}^{+T} - \mathbf{F}_T \mathbf{G}^{-T}] \boldsymbol{P} + \mathscr{H}. \tag{E.7}$$

Notice [from (D.2)] that

$$[\mathbf{G}^+ - \mathbf{G}^- \mathbf{F}_T] \boldsymbol{\Omega} = \boldsymbol{V}_{CM/c} + \boldsymbol{V}_{p/CM} \tag{E.8}$$

gives the velocity of the point of impulse application, relative to the post-ST contact point. By inspection of Fig. 5, then,

$$[\mathbf{G}^+ - \mathbf{G}^- \mathbf{F}_T] = \begin{bmatrix} (l-R)\sin\alpha & (l-R)\sin\alpha & 0 \\ R+(l-R)\cos\alpha & -R-(l-R)\cos\alpha & 0 \end{bmatrix}. \tag{E.9}$$

Also notice that the matrix multiplying $\boldsymbol{\Omega}^+$ is just $\mathbf{M}_T$ as given by (D.10). The matrix multiplying $\boldsymbol{\Omega}^-$ is new. Define

$$I_C^- \equiv m_{\text{leg}}(r_{\text{gyr}}^2 + w^2 - (l-c)((c-R) + R\cos\alpha) + Rw\sin\alpha) \tag{E.10}$$

$$\begin{aligned} I_{FC}^- \equiv\ & 2m_{\text{leg}}((R-l)(R-c)\cos 2\alpha + [l-R+R(c-R)]\cos\alpha + R) \\ & + m_T((l-R)^2\cos 2\alpha + 2(l-R)R\cos\alpha + R^2) \end{aligned} \tag{E.11}$$

$$I_{TC}^- \equiv m_T c_T (R\cos\theta_T + (l-R)\cos(\alpha+\theta_T)) \tag{E.12}$$

$$I_F^- \equiv m_{\text{leg}}(r_{\text{gyr}_F}^2 + (l-c)(R-c) + w^2) - m_{\text{leg}} R((l-c)\cos\alpha + w\sin\alpha) \tag{E.13}$$

$$I_{TF}^- \equiv m_T c_T (R\cos\theta_T + (l-R)\cos(\theta_T - \alpha)). \tag{E.14}$$

Then

$$[\mathbf{M}_{T_f}^+ + \mathbf{G}^{+T} \mathbf{G}^- \mathbf{F}_T] = \begin{bmatrix} I_C^- & I_{FC}^- & I_{TC}^- \\ 0 & I_F^- & 0 \\ 0 & I_{TF}^- & I_T \end{bmatrix}. \tag{E.15}$$

It remains to choose $\mathscr{H}$ such that the $\Omega_T^+ = 0$. Thus, solving the third eqn of (E.7) for the necessary torsional impulse gives

$$\mathscr{H} = I_{TC}\Omega_C^+ - I_{TF}^-\Omega_F^-. \tag{E.16}$$

This is applied by reaction against the post-ST stance leg; thus putting $-\mathscr{H}$ into the first equation of (E.7) leads to the following 2×2 system for Ω_C and Ω_F:

$$\mathbf{M}^+\boldsymbol{\Omega}^+ = \mathbf{M}^-\boldsymbol{\Omega}^- + \begin{bmatrix} (l-R)\sin\alpha & R+(l-R)\cos\alpha \\ (l-R)\sin\alpha & -R-(l-R)\cos\alpha \end{bmatrix} \boldsymbol{P} \tag{E.17}$$

$\mathbf{M}^+$ is as given by (D.23), and

$$\mathbf{M}^- \equiv \begin{bmatrix} I_C^- & I_{FC}^- + I_{TF}^- \\ 0 & I_F^- \end{bmatrix}. \tag{E.18}$$

Solving for $\boldsymbol{\Omega}^+$ leads to the support transfer eqn (76) given in section 8, with

$$\boldsymbol{\Lambda} \equiv \mathbf{M}^{+-1}\mathbf{M}^- \begin{bmatrix} 0 & 1 \\ 1 & 0 \end{bmatrix} \tag{E.19}$$

$$\boldsymbol{\Gamma} \equiv \mathbf{M}^{+-1} \begin{bmatrix} (l-R)\sin\alpha & R+(l-R)\cos\alpha \\ (l-R)\sin\alpha & -R-(l-R)\cos\alpha \end{bmatrix}. \tag{E.20}$$

APPENDIX F

Linearization of the Stride Function

For the purposes of linearization it is convenient to write the stride function (77) in the form

$$f = \begin{bmatrix} \mathbf{D}_{\theta\theta} & \mathbf{D}_{\theta\Omega} \\ \boldsymbol{\Lambda}\mathbf{D}_{\Omega\theta} & \boldsymbol{\Lambda}\mathbf{D}_{\Omega\Omega} \end{bmatrix} \begin{bmatrix} \lambda\alpha_k - \Delta\boldsymbol{\theta}_{SE} \\ \boldsymbol{\Omega}_k \end{bmatrix} + \begin{bmatrix} \Delta\boldsymbol{\theta}_{SE} \\ \boldsymbol{\Gamma}\boldsymbol{P}_{k+1} \end{bmatrix} - \begin{bmatrix} -\lambda\alpha_{k+1} \\ \boldsymbol{\Omega}_{k+1} \end{bmatrix}. \tag{F.1}$$

Then the linearized stride function (90) emerges from

$$\begin{bmatrix} \Delta\alpha_{k+1} \\ \Delta\Omega_{C_{k+1}} \\ \Delta\Omega_{Fk+1} \\ \Delta\tau_k \end{bmatrix} = -\begin{bmatrix} \dfrac{\partial f}{\partial\alpha_{k+1}} & \dfrac{\partial f}{\partial\Omega_{C_{k+1}}} & \dfrac{\partial f}{\partial\Omega_{Fk+1}} & \dfrac{\partial f}{\partial\tau_k} \end{bmatrix}^{-1} \begin{bmatrix} \dfrac{\partial f}{\partial\alpha_k} & \dfrac{\partial f}{\partial\Omega_{C_k}} & \dfrac{\partial f}{\partial\Omega_{Fk}} & \dfrac{\partial f}{\partial P_{x_{k+1}}} & \dfrac{\partial f}{\partial P_{y_{k+1}}} \end{bmatrix} \begin{bmatrix} \Delta\alpha_k \\ \Delta\Omega_{C_k} \\ \Delta\Omega_{Fk} \\ \Delta P_{x_{k+1}} \\ \Delta P_{y_{k+1}} \end{bmatrix}. \tag{F.2}$$

Calculation of the partials of f is straightforward given the partials of the various component matrices. Actually most of the component partials are zero; only the following three are not.

(i) $\partial \mathbf{D}/\partial \tau_k$

The equations of motion (72) can be written (with T excluded) in the form

$$\frac{\mathrm{d}}{\mathrm{d}t}\begin{bmatrix}\Delta\boldsymbol{\theta}-\Delta\boldsymbol{\theta}_{SE}\\ \boldsymbol{\Omega}\end{bmatrix}=\begin{bmatrix}\mathbf{0} & \mathbf{I}\\ -\mathbf{M}_0^{-1}\mathbf{K} & \mathbf{0}\end{bmatrix}\begin{bmatrix}\Delta\boldsymbol{\theta}-\Delta\boldsymbol{\theta}_{SE}\\ \boldsymbol{\Omega}\end{bmatrix}$$

$$=\boldsymbol{\Phi}\mathbf{Q}\boldsymbol{\Phi}^{-1}\begin{bmatrix}\Delta\boldsymbol{\theta}-\Delta\boldsymbol{\theta}_{SE}\\ \boldsymbol{\Omega}\end{bmatrix} \tag{F.3}$$

where $\mathbf{Q}$ is the diagonal matrix of eigenvalues, and $\boldsymbol{\Phi}$ the matrix of corresponding eigenvectors. The transition matrix $\mathbf{D}$ is then

$$\mathbf{D}(\tau_k)=\boldsymbol{\Phi}\, e^{\mathbf{Q}\tau_k}\,\boldsymbol{\Phi}^{-1}. \tag{F.4}$$

The derivative of $\mathbf{D}$ is therefore

$$\frac{\partial \mathbf{D}}{\partial \tau_k}=\boldsymbol{\Phi}\mathbf{Q}\, e^{\mathbf{Q}\tau_k}\,\boldsymbol{\Phi}^{-1}=(\boldsymbol{\Phi}\mathbf{Q}\boldsymbol{\Phi}^{-1})(\boldsymbol{\Phi}\, e^{\mathbf{Q}\tau_k}\,\boldsymbol{\Phi}^{-1})=\begin{bmatrix}\mathbf{0} & \mathbf{I}\\ -\mathbf{M}_0^{-1}\mathbf{K} & \mathbf{0}\end{bmatrix}\mathbf{D}. \tag{F.5}$$

(ii) $\partial \boldsymbol{\Lambda}/\partial \alpha_{k+1}$

Differentiating (E.19) involves

$$\frac{\partial(\mathbf{M}^{+^{-1}}\mathbf{M}^-}{\partial\alpha}=\frac{\partial \mathbf{M}^{+^{-1}}}{\partial\alpha}\mathbf{M}^-+\mathbf{M}^{+^{-1}}\frac{\partial \mathbf{M}^-}{\partial\alpha}. \tag{F.6}$$

But

$$\frac{\partial \mathbf{M}^{+^{\ 1}}}{\partial\alpha}=-\mathbf{M}^{+^{-1}}\frac{\partial \mathbf{M}^+}{\partial\alpha}\mathbf{M}^{+^{-1}}. \tag{F.7}$$

So

$$\frac{\partial \boldsymbol{\Lambda}}{\partial\alpha}=\mathbf{M}^{+^{-1}}\left(\frac{\partial \mathbf{M}^-}{\partial\alpha}\begin{bmatrix}0 & 1\\ 1 & 0\end{bmatrix}-\frac{\partial \mathbf{M}^+}{\partial\alpha}\boldsymbol{\Lambda}\right) \tag{F.8}$$

$\partial \mathbf{M}^+/\partial\alpha$ and $\partial \mathbf{M}^-/\partial\alpha$ are found directly by differentiating the elements of (D.23) and (E.18), respectively, and evaluating at $\theta_C=-\alpha_0$, $\theta_F=\pi+\alpha_0$. Notice that $\mathrm{d}\theta_C/\mathrm{d}\alpha=-1$, $\mathrm{d}\theta_F/\mathrm{d}\alpha=1$.

(iii) $\partial \boldsymbol{\Gamma}/\partial \alpha_{k+1}$

From (E.20), and by analogy with (F.8),

$$\frac{\partial \boldsymbol{\Gamma}}{\partial\alpha}=\mathbf{M}^{+^{\ 1}}\left(\begin{bmatrix}(l-R)\cos\alpha & -(l-R)\sin\alpha\\ (l-R)\cos\alpha & (l-R)\sin\alpha\end{bmatrix}-\frac{\partial \mathbf{M}^+}{\partial\alpha}\boldsymbol{\Gamma}\right) \tag{F.9}$$

(F.5), (F.8), and (F.9) are evaluated at the steady cycle conditions, and inserted into the appropriate slots of (F.2). The "ΔP-controlled" stride-to-stride eqns (90) result.

APPENDIX G

Recasting in Terms of ΔW

As discussed in section 12, in practice it may prove most convenient to specify the impulsive push by the energy delivered W and the angle of application $(\alpha+\phi_p)$. To

reformulate the linearization in terms of these variables, differentiate (87) as follows:

$$\begin{aligned} dW = {} & \boldsymbol{P}_0^T[\mathbf{I}+\mathbf{G}\mathbf{M}_f^{-1}\mathbf{G}^T]\,d\boldsymbol{P} \\ & +\tfrac{1}{2}\boldsymbol{P}_0^T[d\mathbf{G}\,\mathbf{M}_f^{-1}\mathbf{G}^T+\mathbf{G}\mathbf{M}_f^{-1}d\mathbf{G}^T-\mathbf{G}\mathbf{M}_f^{-1}\,d\mathbf{M}_f\,\mathbf{M}_f^{-1}\mathbf{G}^T]\boldsymbol{P}_0. \end{aligned} \tag{G.1}$$

Now write $\boldsymbol{P}$ as

$$\boldsymbol{P} = P\begin{bmatrix}\cos(\alpha+\phi_p)\\ \sin(\alpha+\phi_p)\end{bmatrix} \equiv P\boldsymbol{p}. \tag{G.2}$$

Then the differential of $\boldsymbol{P}$ is

$$d\boldsymbol{P} = d\boldsymbol{P}\boldsymbol{p} + P\,d\boldsymbol{p}. \tag{G.3}$$

To get $d\boldsymbol{P}$, return to the energy formula (G.1). In terms of $(P, \boldsymbol{p})$ it becomes

$$\begin{aligned} dW = {} & \boldsymbol{P}_0^T[\mathbf{I}+\mathbf{G}\mathbf{M}_f^{-1}\mathbf{G}^T]\boldsymbol{p}\,dP + \boldsymbol{P}_0^T[\mathbf{I}+\mathbf{G}\mathbf{M}_f^{-1}\mathbf{G}^T]P\frac{\partial \boldsymbol{p}}{\partial \phi_p}\,d\phi_p \\ & + \boldsymbol{P}_0^T\Bigg([\mathbf{I}+\mathbf{G}\mathbf{M}_f^{-1}\mathbf{G}^T]P\frac{\partial \boldsymbol{p}}{\partial \alpha} \\ & + \frac{1}{2}\left[\frac{\partial \mathbf{G}}{\partial \alpha}\mathbf{M}_f^{-1}\mathbf{G}^T+\mathbf{G}\mathbf{M}_f^{-1}\frac{\partial \mathbf{G}^T}{\partial \alpha}-\mathbf{G}\mathbf{M}_f^{-1}\frac{\partial \mathbf{M}_f}{\partial \alpha}\mathbf{M}_f^{-1}\mathbf{G}^T\right]\boldsymbol{P}_0\Bigg)\,d\alpha. \end{aligned} \tag{G.4}$$

Solving for dP leaves an expression of the form

$$dP = \frac{\partial P}{\partial \alpha}\,d\alpha + \frac{\partial P}{\partial W}\,dW + \frac{\partial P}{\partial \phi_p}\,d\phi_p. \tag{G.5}$$

Putting this into (G.3) produces gradients of $\boldsymbol{P}_{k+1}$, in the form

$$\begin{bmatrix} \dfrac{\partial P_{x_{k+1}}}{\partial \alpha_{k+1}} & \dfrac{\partial P_{x_{k+1}}}{\partial W_{k+1}} & \dfrac{\partial P_{x_{k+1}}}{\partial \phi_{p_{k+1}}} \\ \dfrac{\partial P_{y_{k+1}}}{\partial \alpha_{k+1}} & \dfrac{\partial P_{y_{k+1}}}{\partial W_{k+1}} & \dfrac{\partial P_{y_{k+1}}}{\partial \phi_{p_{k+1}}} \end{bmatrix}. \tag{G.6}$$

Inserting this in turn into (F.2) converts from "$\Delta\boldsymbol{P}$-controlled" stride-to-stride eqn (90) to "ΔW-controlled" eqn (91).